Chem Soc Rev

REVIEW ARTICLE

View Article Online
View Journal | View Issue

CrossMark click for updates

Cite this: *Chem. Soc. Rev.*, 2015, 44, 2998

Towards single molecule switches

Jia Lin Zhang,[ab] Jian Qiang Zhong,[ab] Jia Dan Lin,[ab] Wen Ping Hu,[c] Kai Wu,[de] Guo Qin Xu,[adf] Andrew T. S. Wee[b] and Wei Chen*[abdf]

The concept of using single molecules as key building blocks for logic gates, diodes and transistors to perform basic functions of digital electronic devices at the molecular scale has been explored over the past decades. However, in addition to mimicking the basic functions of current silicon devices, molecules often possess unique properties that have no parallel in conventional materials and promise new hybrid devices with novel functions that cannot be achieved with equivalent solid-state devices. The most appealing example is the molecular switch. Over the past decade, molecular switches on surfaces have been intensely investigated. A variety of external stimuli such as light, electric field, temperature, tunneling electrons and even chemical stimulus have been used to activate these molecular switches between bistable or even multiple states by manipulating molecular conformations, dipole orientations, spin states, charge states and even chemical bond formation. The switching event can occur either on surfaces or in break junctions. The aim of this review is to highlight recent advances in molecular switches triggered by various external stimuli, as investigated by low-temperature scanning tunneling microscopy (LT-STM) and the break junction technique. We begin by presenting the molecular switches triggered by various external stimuli that do not provide single molecule selectivity, referred to as non-selective switching. Special focus is then given to selective single molecule switching realized using the LT-STM tip on surfaces. Single molecule switches operated by different mechanisms are reviewed and discussed. Finally, molecular switches embedded in self-assembled monolayers (SAMs) and single molecule junctions are addressed.

Received 8th November 2014

DOI: 10.1039/c4cs00377b

www.rsc.org/csr

Open Access Article. Published on 11 March 2015. Downloaded on 6/24/2024 3:25:25 PM. This article is licensed under a Creative Commons Attribution 3.0 Unported Licence.

1. Introduction of molecular switches on surfaces

In the early 1970s, the visionary concept of using individual molecules as active electronic components was sketched out by Arieh Aviram and Mark Ratner.[1] Since then, molecular electronics has been considered one possible revolutionary successor to conventional semiconducting electronics.[2–4] Research efforts have been devoted to exploring the properties and device opportunities of single molecules.[5–16] However, the rapid development of molecular electronics only really took off during the past two decades in tandem with the rise of the nanoscience era and the availability of manipulation probes at the single molecule scale, such as the scanning tunneling microscope, mechanically controlled break junction (MCBJ) or electromigration break junction (EBJ) techniques.[17–23] Initially, miniaturization and cost reduction were the main driving forces that provided the impetus to develop a variety of experimental platforms to probe electronic transport phenomena at the single molecule level.[24–26] Significant advances have been achieved over the past several years. Although it is tempting to use molecular electronics to mimic the basic functions of silicon devices, these approaches do not really tap the potential of molecules. The field of molecular electronics would only mature if it moves beyond the paradigm of conventional electronics and simple transport models, and instead explores the intrinsic functionality of molecules.[27–33] Indeed, contemporary research in molecular electronics is already moving in this direction.

Molecules often possess unique properties that have no parallel in conventional materials, such as monodispersity, self-assembly ability, intrinsic quantum mechanical behavior, functionality and the ease of replacing functional groups, flexible and low cost solution synthesis, *etc.* Therefore, the rational design of molecules with specific functionality promises new devices with functions that cannot be achieved with

[a] *Department of Chemistry, National University of Singapore, 3 Science Drive 3, 117543, Singapore*
[b] *Department of Physics, National University of Singapore, 2 Science Drive 3, 117542, Singapore. E-mail: phycw@nus.edu.sg*
[c] *School of Science, Tianjin University, Tian Jin, 300072, China*
[d] *Singapore-Peking University Research Center for a Sustainable Low-Carbon Future, 1 CREATE Way, CREATE Tower, Singapore 138602, Singapore*
[e] *College of Chemistry and Molecular Engineering, Peking University, Beijing 100871, China*
[f] *National University of Singapore (Suzhou) Research Institute, 377 Lin Quan Street, Suzhou Industrial Park, Jiang Su 215123, China*

This journal is © The Royal Society of Chemistry 2015

Open Access Article. Published on 11 March 2015. Downloaded on 6/24/2024 3:25:25 PM.
This article is licensed under a Creative Commons Attribution 3.0 Unported Licence.

equivalent solid-state devices. Novel applications include coupling light to the molecule for optoelectronic devices;[15,34–36] harnessing the electromechanical properties for molecular machines;[37–39] manipulating the electron spin for memory devices or spintronic devices;[23,40–47] and utilizing the unique recognition properties for molecular sensors.[48–50] The most appealing and basic example of a functional molecule is the molecular switch.

Over the years, molecular switches on surfaces have been intensely investigated.[51–96] A variety of external stimuli such as light,[72,79] electric field,[52,66] temperature[70] and tunneling electrons[53–59,68,73,75,77,78] can be used to activate these molecular switches between bistable[51–58] or even multiple states.[77,78] Depending on the properties of the molecules, they can be switched by changing conformations,[52–57,64–67,69–72,77–81] dipole orientations,[97,98] spin states,[74,75] charge states,[58–61,63] or even bond formation.[62] For such molecules to be used as electronic components, they should be coupled to a support substrate and wired to a molecular circuit without suppressing their switching performance. Self-assembly represents a promising bottom up approach to integrate these molecules into circuits on surfaces.[99] Single molecular switches can also be chemically connected to one or two external electrodes by the break junction techniques, such as STM-based break junctions, MCBJs and EBJs. Single molecular diode or single molecule field-effect transistor behavior can be realized in the break junction configurations.

In this review article, we highlight recent advances in molecular switches triggered by various external stimuli and realized in different configurations. We begin by presenting molecular switches on surfaces triggered by various external stimuli that do not provide single molecule selectivity, referred to as non-selective switching. Special focus is then given to single molecule manipulation realized using low-temperature scanning tunneling microscopy (LT-STM), which offers unique opportunities to operate individual switches on the atomic scale. The conductance switching of the oligo(phenylene-ethynylene)s (OPEs) within SAMs are also discussed. In the end, single molecule switches developed using break junction techniques are demonstrated.

2. Non selective switching triggered by various external stimuli

Molecular switches, which can be interconverted between bistable or even multiple states by external stimuli such as light,[72,79] electric field,[42,56] temperature,[70] electrons[53–59,68,73,75,77,78] or even chemical modifications,[100,101] have attracted much attention. These external stimuli do not usually provide single molecule selectivity (except the tunneling electrons from a STM tip). Most switching processes are studied by LT-STM due to its atomic-scale imaging capability. Hence, both the local topography and electronic configurations can be probed before and after the switching. Atomic scale characterization can provide a fundamental understanding of the interaction between the molecule and the external stimuli, and also help find a better way to engineer the functionality of the molecule from rational chemical design. In the following sub-sections, we will introduce the various external stimuli in more detail.

2.1 Light induced switching

Photochromic systems can convert photon energy into mechanical energy; thus they can be used as building blocks for the fabrication of molecular device prototypes based on photomechanical effects. Among photochromic molecules, azobenzenes have been extensively investigated due to their photoisomerization property.[66,69,72,102–107] They can reversibly transform from one isomeric state to another upon adsorption of light in the gas-phase or solution-phase. However, this process can be quenched at a surface due to the molecule-surface coupling. By attaching four *tert*-butyl ''legs'' (TB: C_4H_9) to an azobenzene scaffold ($C_{12}H_{10}N_2$), Comstock *et al.* demonstrated reversible light-induced mechanical switching between *trans* and *cis* states on Au(111).[72] The TB legs lift the azobenzene molecule from the substrate, thereby increasing molecular photomechanical activity by reducing the molecule-surface coupling. Fig. 1a and b shows the same island of TTB-azobenzene molecules on Au(111) before and after a 3 h exposure to UV light. Before UV

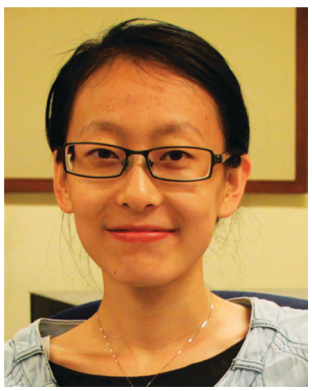

Jia Lin Zhang

Jia Lin Zhang received her Bachelor's degree in Physics from Sichuan University in 2010 and PhD degree from the Physics Department at the National University of Singapore (NUS) in 2014. She is currently a postdoctor research fellow in the Chemistry Department at NUS. Her research interests include molecular self-assembly, single molecule manipulation and two-dimensional material growth.

Wei Chen

Dr Wei Chen is currently an Associate Professor in both the Chemistry Department and Physics Department at the National University of Singapore (NUS). He received his Bachelor's degree in Chemistry from Nanjing University (China) in 2001 and PhD degree from Chemistry Department at NUS in 2004. His current research interests include Molecular-scale Interface Engineering for Molecular, Organic and Graphene Electronics, and Interface-Controlled Nanocatalysis for Energy and Environmental Research.

Open Access Article. Published on 11 March 2015. Downloaded on 6/24/2024 3:25:25 PM.
This article is licensed under a Creative Commons Attribution 3.0 Unported Licence.

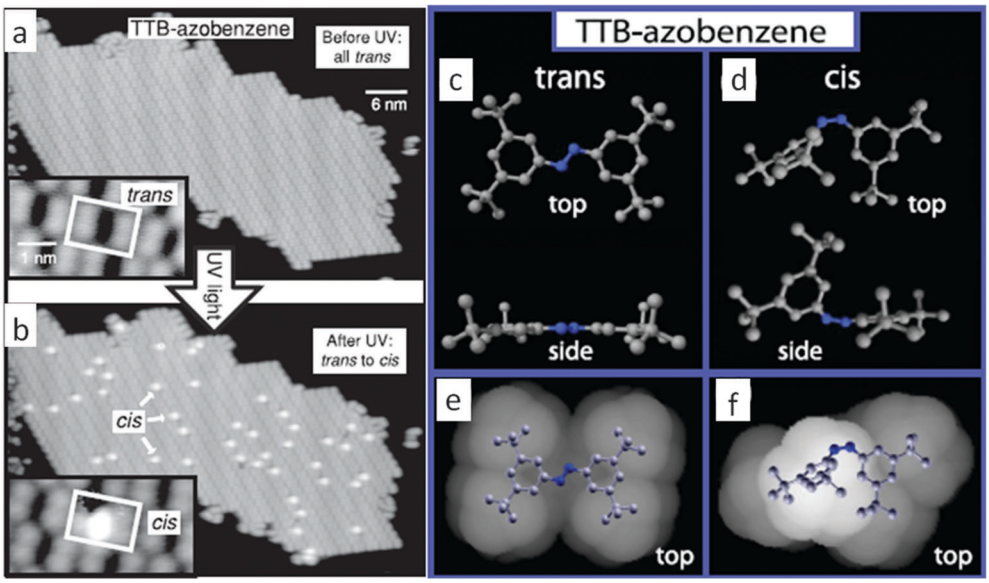

Fig. 1 (a) Same island of TTB-azobenzene molecules before and (b) after a 3 h exposure to 90 mW cm^{-2} UV irradiation at 375 nm. (c) Calculated *trans* geometry. (d) Calculated *cis* geometry. (e) Calculated *trans* LDOS integrated from E_F to $E_F - 1$ eV, at an isosurface about 3 Å away from the nearest atoms. (f) Calculated *cis* LDOS isosurface. Reprinted from ref. 72, with permission from the American Physical Society, copyright 2007.

exposure the island is uniformly composed of the *trans*-isomer with four peripheral lobes. After UV exposure the emergence of the *cis* isomer of TTB-azobenzene (bright protrusions) can be seen in the island. The calculated geometry and local density of states (LDOS) isosurface integrated from E_F to $E_F - 1$ eV for *trans* and *cis* azobenzenes are shown in Fig. 1c–f, in good agreement with the experiment. Theoretical studies suggest that there are two possible mechanisms for the *trans–cis* switching in solution. One is the inversion mechanism with in-plane bending of the C–N=N angle,[104] another is the rotation mechanism, with an out-of-plane rotation of the N=N bond.[108] However, for the metallic surface-bond azobenzene, the switching is proposed *via* the formation of a hole in the d band of the metal surface and subsequent transfer of an electron from the HOMO.[109] The azobenzene molecules adsorbed on the surface have a low photoswitching efficiency compared with that in solution. Many applications profiting from the conformational rearrangement of the molecule have been proposed, such as optical data storage devices, sensors and light-powered molecular machines.[110–112]

2.2 Electric field induced switching

Another way to induce molecular switching is the use of an electric field. In the presence of an electric field, the reaction potential energy pathway can be deformed, leading to an effective lowering of the switching barrier. This effect depends on the presence and orientation of an intrinsic dipole moment, as well as the polarizability of the molecule.[52] Using the same azobenzene molecule as in Section 2.1, Alemani *et al.* demonstrated an electric field induced reversible *trans–cis* isomerization by STM.[66] The isomerization experiments were performed by positioning the STM tip at a fixed height above a molecular island with the feedback loop off and applying a pulse voltage V to the centre of the island. The STM images before and after nine equivalent pulses are shown in Fig. 2a and b. Many molecules have changed their appearance from the *trans* form to the *cis* form. It is found that the threshold voltage increases when retracting the tip. The isomerization process occurs even at very large sample-tip distances where no tunneling current is flowing. Moreover, it is also possible to isomerize molecules when the tip is positioned above the bare surface near the molecular island. All these observations, together with the large distance over which switched molecules are observed, lead to the conclusion that the *trans–cis* isomerization is driven by the electric field in the STM junction. Comparison of the light induced and electric field induced switching shows that different external stimuli can be used to operate the very same molecule.

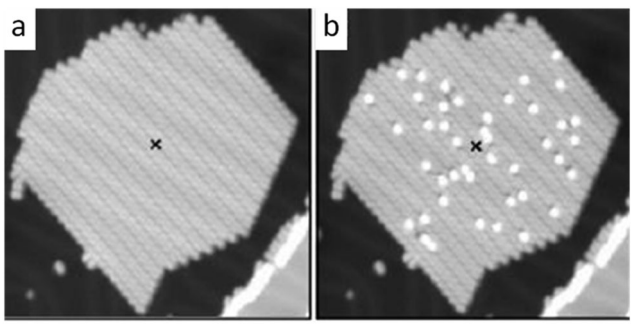

Fig. 2 (a) Island of *trans*-TBA containing about 400 molecules (37 × 37 nm^2). Subsequent voltage pulses (20 s, V_{sample} = 2 V, tip height = 6 Å) are applied at the position indicated by the cross. (b) STM image after nine pulses: 43 molecules have been switched to the *cis* form. Reprinted from ref. 66, with permission from the American Chemical Society, copyright 2006.

2.3 Temperature induced switching

In some molecular systems, the energy barrier between two molecular states is relatively low (about kT or 0.026 eV). In that case, it

 This journal is © The Royal Society of Chemistry 2015

Open Access Article. Published on 11 March 2015. Downloaded on 6/24/2024 3:25:25 PM.
This article is licensed under a Creative Commons Attribution 3.0 Unported Licence.

is possible to switch a molecule by thermal excitation. Such temperature induced switching is, however, not very directional. Switching can occur in both directions unless there is a significant energy difference between the two isomers of the molecules. Weigelt *et al.* investigated a model system with thermally induced conformational changes.[80] The chemical structure of the investigated molecule 1,4-bis[(5-*tert*-butyl-3-formyl-4-hydroxyphenyl)ethynyl]benzene is shown in Fig. 3a. Vapor deposition of this compound onto the inert herringbone reconstructed Au(111)-(22 × $\sqrt{3}$) surface results in two coexisting adsorption phases. In the phase shown in Fig. 3c, the molecules adsorb with their backbone parallel to the substrate and align into rows shifted relative to each other by half the repeat distance along the rows, analogous to the stacking in a brick wall. As shown in Fig. 3b, three surface conformers exist: one achiral *meso*-form (LR/RL) and two chiral enantiomers (LL and RR). From the time-lapse sequence of STM images, it is found that the bright protrusions ascribed to *t*-butyl groups occasionally change position from one side of the molecular backbone to the other. Such shifts are illustrated in Fig. 3d by superimposing two time-separated STM images of the same surface area. This spontaneous flipping process implies that the molecules can switch between different surface conformations, specifically from chiral (RR/LL) to achiral (RL/LR) or *vice versa*. The observed conformational changes have implications for the chiral ordering on surfaces. As shown by the coexisting second phase in Fig. 3e, the molecules connect to form two windmill-like arrangements with different chirality. Each chiral form of the tilting pattern consists entirely of one of the two chiral surface conformers (LL/RR). The homochiral assembly on surfaces is of interest in heterogeneous asymmetric catalysis.

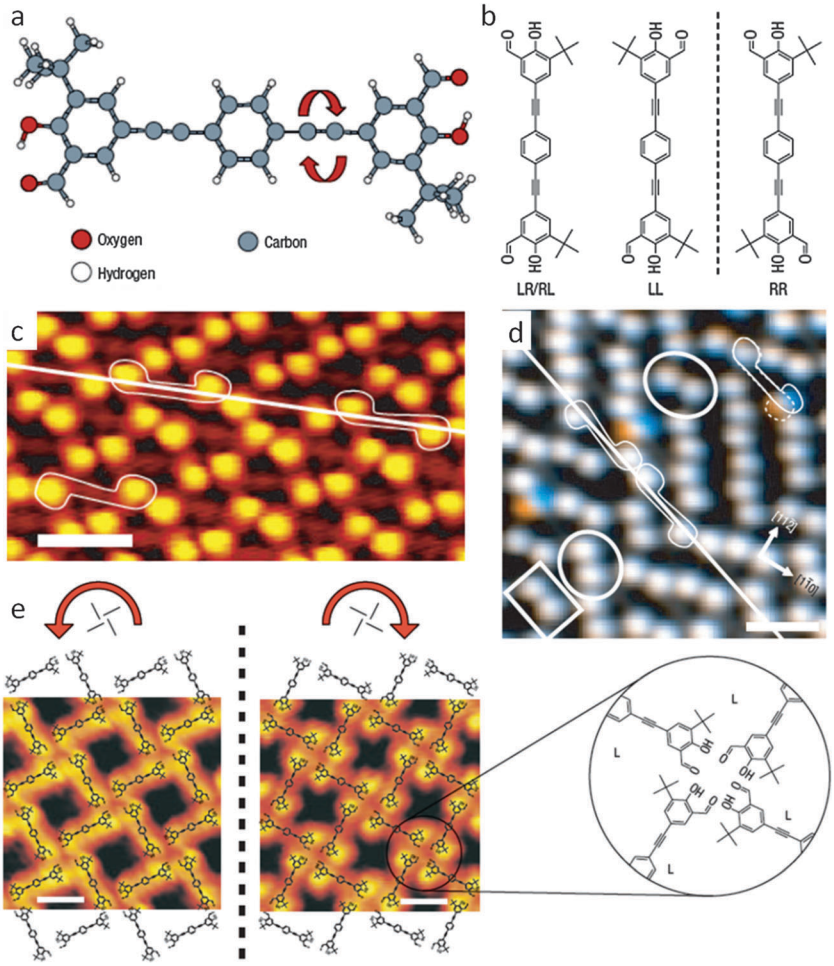

Fig. 3 (a) Chemical structure of the investigated molecule 1,4-bis[(5-*tert*-butyl-3-formyl-4-hydroxyphenyl)ethynyl]benzene. (b) Three distinct surface conformers, two of which are enantiomers. R and L indicate the position (right and left) of the *t*-butyl group with respect to the molecular backbone as seen from the centremost benzene ring. (c) Constant current STM image of the brick-wall adsorption structure attained under tip conditions primarily revealing the *t*-butyl groups. (d) Overlay of two STM images taken with a time separation of 168 s (V_{sample} = 1.96 V, I = 0.4 nA, T_{sample} = 180 K, scale bar 2 nm). Blue (orange) indicates the initial (final) positions of *t*-butyl groups that change position, whereas stationary groups appear grey. Two *cis*–*trans* and one *trans*–*cis* (right most in image) flips are shown. Outlines of three molecules are indicated as well as stationary *cis* (rectangle) and *trans* (circles) arrangements of endgroups. The indicated line follows the direction of the molecular backbones. (e) STM images and schematic models of the network structure (scale bar 2 nm). The images show domains of opposite chirality. The zoom-in on a structural node illustrates the correlation between the tiling pattern and the molecular chirality, leading to homochiral domains consisting exclusively of RR or LL-conformers. Reprinted from ref. 80, with permission from Nature Publishing Group, copyright 2006.

Open Access Article. Published on 11 March 2015. Downloaded on 6/24/2024 3:25:25 PM.
This article is licensed under a Creative Commons Attribution 3.0 Unported Licence.

2.4 Tunneling electron induced switching

There has been much effort to understand the interactions between electrons and adsorbates on surfaces. Different mechanisms can be involved, including desorption induced by electron transitions,[113] direct coherent excitation induced desorption,[114] resonant electron stimulated desorption,[115] desorption induced by multiple electron transitions and dissociative electron attachments.[116,117] However, the surface phenomena are not limited to desorption. Using tunneling electrons, various modifications of the adsorbates, which cannot be obtained with conventional sources, have been observed by STM.[85,86,88] Surface phenomena such as desorption,[118] dissociation,[119] hopping,[120] rotation[121] and chemical reactions[122] have been reported as a consequence of electronic or vibrational excitation. By injecting hot electrons from an STM tip, Chen *et al.* demonstrated the nonlocal chemical reactivity of one monolayer copper hexadecafluorophthalocyanine (F_{16}CuPc) adsorbed on two different substrates, Ag(111) and Au(111).[123]

Fig. 4a and b show the STM images of F_{16}CuPc molecules adsorbed on the Ag(111) and Au(111) surface before pulsing. After applying a pulse on the target molecule on Ag(111), one of the four ligands of the molecule disappears. Such a chemical reaction is not limited to the molecule under the STM tip. As shown in Fig. 4c (pulsed at −3.0 V tip bias, 3.5 nA, 50 ms), the reaction also occurs on five molecules at different distances from the STM tip. This nonlocal chemical reaction can be observed as far as 12 nm from the STM tip. Similar nonlocal behavior is also observed for molecules on Au(111), where one ligand of the reacted molecules is shortened by the pulse (Fig. 4d). The threshold voltage for this nonlocal chemical reaction is determined to be −1.9 V and −2.4 V for Ag(111) and Au(111) respectively. The relatively high energy suggests that the reaction proceeds *via* electronic excitations of the molecule. If the reaction is induced by tunneling electrons, the reaction rate R_0, current I_0 and reaction order n should obey the relation $R_0 = I_0^n$.[88] By investigating the switching rate as a function of the tunneling current, the reaction order is deduced to be ∼4 (∼2) for Ag (Au), and the single-molecule reaction deduced to be a four-electron (two-electron) process for molecules on Ag(111) (Au(111)). The observed shorter ligand is caused by C–F bond dissociation. The mechanism is known as dissociative electron attachment,[124] in which electrons with specific energies can be captured into the antibonding π* orbitals of the molecule, and then transferred into the σ* orbital, causing bond breaking. Lateral hot-electron propagation is proposed to explain the nonlocal reactions. Density functional theory (DFT) calculations reveal that the mixing of molecular orbitals with metal surface states is the main channel facilitating the propagation of hot electrons, as shown in the schematic in Fig. 4e and f. Electrons propagating in a metal surface can back-transfer into the π* orbitals of another molecule through the "bridge" formed between the molecule and substrate, leading to another defluorination reaction.

In addition to the bistable switching, the tunneling electrons can also trigger multi-state switching. Elegant examples include the tunneling electron induced rotation of a triangular Sc_3N cluster within an icosahedral C_{80} fullerene cage among three different configurations, where the antisymmetric stretch vibration of Sc_3N acts as the gateway for energy transfer;[125] and a four-level conductance switching of the free-base tetraphenylporphyrin molecule by tunneling electron induced moving of the inner hydrogen atom between different positions.[78]

2.5 Chemical stimulus induced switching

Planar organometallic complexes with extended π-conjugation, for example, metalloprophyrins and metallophthalocyanines, can possess a wide range of functionalities.[126–128] Their chemical properties can be varied by changing the metal ion at the center or by attaching different functional groups to the macrocycle. Moreover, the coordinatively unsaturated character of the metal center can act as a local reactive site for the ligand attachment, which opens the unique possibility of controlling its properties by external chemical stimuli.[129–132] The coordination of gas molecules to the metal center usually causes measurable changes in the molecule-substrate interaction,[129] color,[49] or even magnetic properties of the metal complex,[133] enabling promising applications

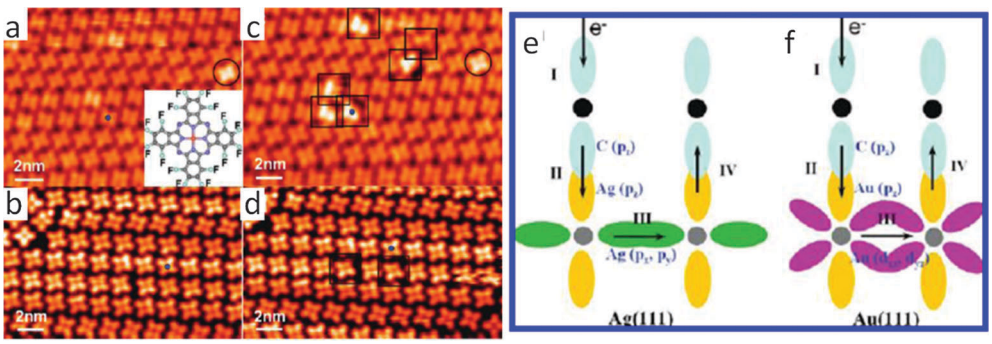

Fig. 4 (a) STM images of F_{16}CuPc molecules adsorbed on Ag(111) surface and (b) Au(111) surface before pulsing. (c) STM images of F_{16}CuPc molecules on Ag(111) and (d) Au(111) after a pulse at −3.0 V and −3.2 V on top of the target molecule. The blue dot, rectangles, and circles represent the pulsing position, reacted molecules, and bright molecules not induced by pulsing. (e) Schematic cartoons illustrating the electron transport process. Electron capture in π* orbitals of molecules (step I), transfer from molecule to surface metal atoms (II), propagation in hybridized states of metal atoms (III), then back capture in π* orbitals of another molecule (IV) on Ag(111) and (f) Au(111). Black and gray solid circles represent C atoms of molecules and metal atoms at the surface. Reprinted from ref. 123, with permission from the American Chemical Society, copyright 2009.

 This journal is © The Royal Society of Chemistry 2015

Open Access Article. Published on 11 March 2015. Downloaded on 6/24/2024 3:25:25 PM.
This article is licensed under a Creative Commons Attribution 3.0 Unported Licence.

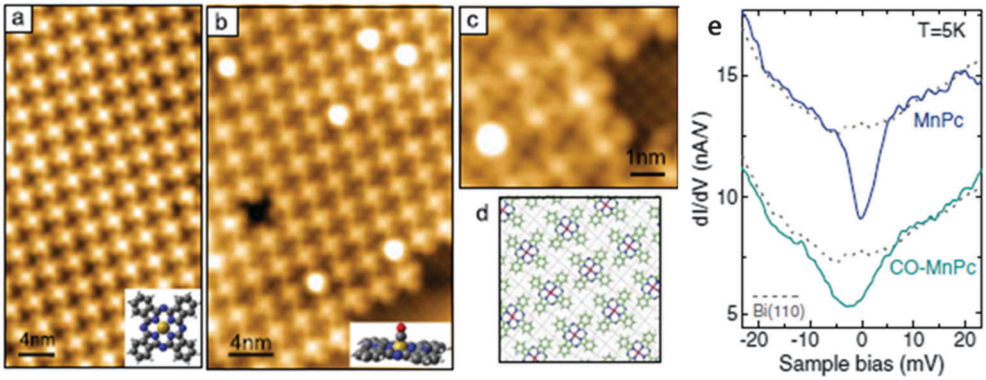

Fig. 5 (a) STM image of a highly ordered MnPc island (V_{sample} = 0.25 V, I = 0.2 nA). (b) MnPc island after exposure to CO (V_{sample} = 0.18 V, I = 0.2 nA). CO-coordianted molecules can be distinguished by different apparent heights. Inset images in (a) and (b) show schematic pictures of the chemical structure of MnPc and CO–MnPc. (c) High resolution STM image of bare and CO-ligated MnPc (V_{sample} = −0.25 V, I = 0.1 nA). (d) Adsorption model of MnPc on Bi(110). (e) dI/dV spectra of MnPc and CO-coordianted MnPc in the bias range close to E_F, showing the zero bias anomaly. The dotted plots are the spectra measured on a bare Bi surface as a reference. Reprinted from ref. 101, with permission from the American Physical Society, copyright 2012.

in gas sensing,[49] catalysis[134] and molecular spintronics.[100] Recently, Stróżecka *et al.* demonstrated chemical control over the molecular spin of manganese phthalocyanine (MnPc) by coordination of CO molecules.[101] Fig. 5a and b shows densely packed MnPc islands on Bi(110) before and after CO exposure. Several molecules exhibiting larger apparent heights in Fig. 5b are identified as CO-ligated MnPc, where a single CO bonds directly to a Mn ion. The corresponding high resolution image is shown in Fig. 5c. The differential conductance (dI/dV) spectrum measured close to E_F on MnPc reveals a pronounced anomaly at zero bias, which is a fingerprint of the Kondo effect (Fig. 5d).[135–138] When similar spectra are measured on CO–MnPc molecules, the zero bias anomaly appears much broader, with a slightly different line shape. This indicates that the coordination to CO modifies the magnetic state of the molecule. DFT calculations reveal that the spin of the MnPc molecule is reduced from S = 3/2 to S = 1 upon adsorption. CO ligation further reduces the spin of MnPc from S = 1 to S = 1/2. CO affects the magnetic state of MnPc in two ways. First, it increases the splitting of the d orbitals, hence leading to the low spin configuration; second, it reduces the coupling of the d orbitals to the substrate. This modification is reversible and can be controlled by selective removal of CO molecules using the STM tip.

A common feature of the above mentioned external stimuli is that they cannot provide single molecule selectivity. Although tunneling electrons from the STM tip can potentially manipulate a single molecule, in the situations discussed, lateral transport of hot electron induces nonlocal reactions. In the next section, we focus on the selective STM tip-assisted single molecule manipulation and switching.

3. Selective single molecule manipulation studied by STM

Since its invention in the early 1980s by G. Binnig and H. Roher, STM has become a powerful tool in real-space atomic-scale imaging of surface structures, as well as in characterization of the electronic and vibrational structures of surface adsorbates.[139–142] The STM also offers the fascinating possibility of single molecule manipulation. Manipulation of molecules may involve a controlled change in their positions, switching between different conformations, electronic and chemical structures, or inducing chemical reactions.[85,86] A variety of tip-molecule interactions can be used in a controlled manner to manipulate single molecules, such as the electric field at the tip-sample junction, tunneling electrons, and tip-molecule interaction forces. With STM, various molecular switches supported on surfaces can be studied at the single molecule level. In the following section, we review STM induced single molecule switches induced by different mechanisms, including conformation switching, dipole switching, spin switching, charge switching and bond switching.

3.1 Conformation switching

Most molecular switches operate by changing conformations.[42–47,54–57,59–62,67–71] A conformational switch is defined as a switchable molecule, which has isomers with different three-dimensional (3D) structures. The switch may take place in the 3D molecular conformation, without a modification of the bond structure. This is called stereoisomerization.[84] Elegant examples include the well-known *trans–cis* isomerization of azobenzene molecules as aforementioned and the mechanically interlocked switches formed by catenanes and rotaxanes.[67]

Isomerization may also take place by a reshuffling of the intermolecular chemical bonds, which is referred to as structural isomerization. An elegant example of structural isomerization is the current-induced hydrogen tautomerization of naphthalocyanine molecule, as demonstrated by Liljeroth *et al.*[53] Fig. 6a shows the dI/dV spectra acquired on an isolated naphthalocyanine molecule adsorbed on a NaCl(100) bilayer on Cu(111). The corresponding STM images and DFT simulated images of the HOMO, LUMO and in gap orbitals are shown in Fig. 6b. It is found that the LUMO image allows for easy determination of the position of the inner hydrogens. The arms with hydrogens show a single-lobe structure at the end, as opposed to the nodal plane along the other two arms. Hydrogen taumerization can be induced by positioning the tip above the

Open Access Article. Published on 11 March 2015. Downloaded on 6/24/2024 3:25:25 PM.
This article is licensed under a Creative Commons Attribution 3.0 Unported Licence.

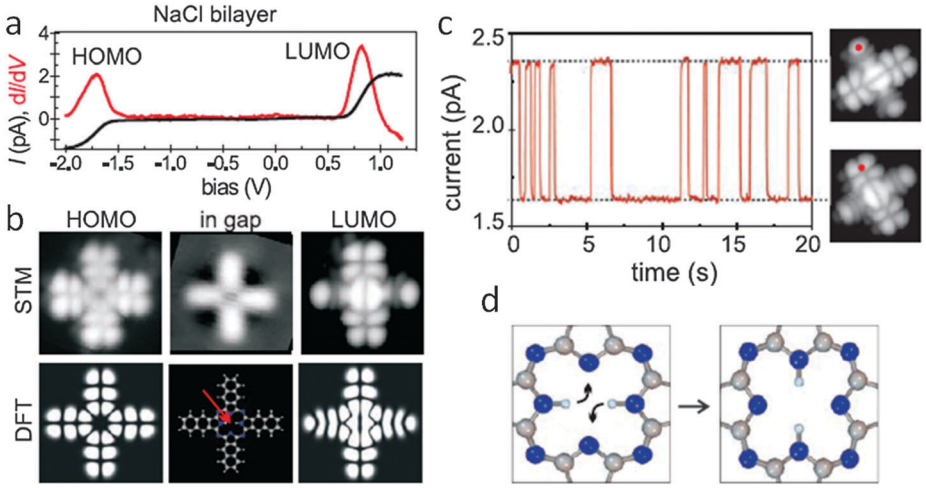

Fig. 6 (a) Spectroscopy of naphthalocyanine on a NaCl bilayer on Cu(111) where the peaks correspond to tunneling into the LUMO (positive bias) and out of the HOMO (negative bias). (b) STM images at V_{sample} = −1.6 V, I = 1 pA (left) and V_{sample} = 0.65 V, I = 1 pA, as well as at low bias (V_{sample} = 0.05 V, I = 1 pA) compared with the calculated HOMO and LUMO of the free molecule. The lower center panel shows the structure model to scale where the arrow indicated the central hydrogen atoms that are along the horizontal arms. The STM images were obtained with a molecule terminated tip. (c) (Left) Current-trace obtained at a bias of 1.7 V when the tip was positioned at one end of the molecule (red dot in STM images). (Right) Orbital images showing the orientation of the LUMO corresponding to the high- or low-current state (2 pA, 0.7 V). (d) Schematic of the hydrogen tautomerization reaction responsible for the switching. Reprinted from ref. 53, with permission from the American Association for the Advancement of Science, copyright 2007.

molecule and substantially increasing the bias above the LUMO resonance. The reaction can be directly monitored in the current signal. During the measurement, the tunneling current switches back and forth between two well defined levels, as shown in Fig. 6c. When the bias is lowered and the LUMO is imaged at resonance, the two current levels correspond to a 90° rotation of the LUMO. This observation is attributed to changes in the position of the imino hydrogens in the central cavity. The dependence of the switching rate on the current is linear. This indicates that the switching is caused by a one-electron process.

3.2 Dipole switching

To enable applications of molecular switches in molecular nanodevices, such as high density data storage devices, it is necessary to introduce the desired functionality into the molecule and assemble them into well-ordered molecular arrays. By rational design of molecules with molecular centers featuring key functionalities such as a dipole or magnetic moment, and peripheral atoms for intermolecular hydrogen bonding, the fabrication of long-range-ordered molecular nanostructure arrays with desired functionalities over macroscopic areas can be achieved.[51,143–146] Dipolar phthalocyanine molecules have been demonstrated to be able to control surface or interface properties and tune the interface energy level alignment in molecule-based devices. Such molecules provide an interesting example of a molecular switch.[143,147–152]

Wang *et al.* have demonstrated a single-dipole molecular switch by pushing and pulling the Sn ion through an adsorbed tin phthalocyanine (SnPc) on Ag(111).[56] As shown in Fig. 7a and b, SnPc can adopt two conformations on Ag(111). In one conformation the Sn atom points toward the vacuum; while in the other conformation, the Sn atom points toward the surface. Molecules directly adsorbed on the metal surface can be transformed

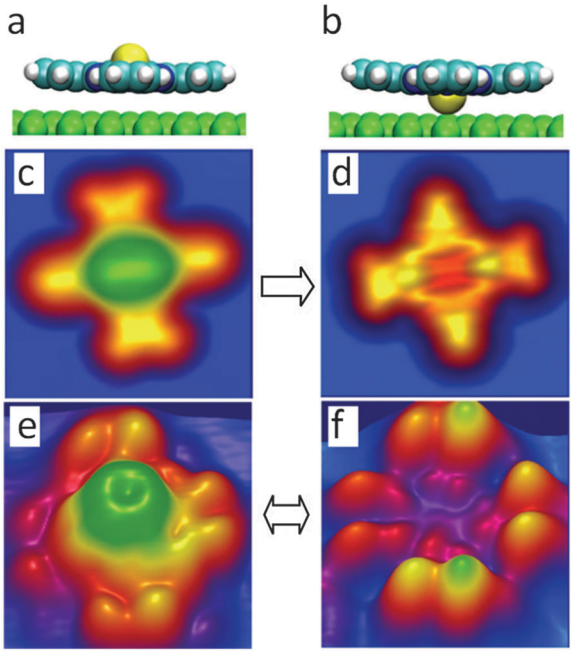

Fig. 7 (a) Side views of Sn-up and (b) Sn-down molecules with fully relaxed adsorption geometry. (c) and (d) pseudo-three-dimensional presentation of constant-current STM images of Sn-up (2.0 × 2.0 nm^2, V_{sample} = −0.2 V, I = 0.05 nA) and Sn-down (2.0 × 2.0 nm^2, V_{sample} = −0.05 V, I = 0.05 nA) molecules adsorbed on Ag(111). (e) and (f) STM images of Sn-up (2.0 × 2.0 nm^2, V_{sample} = −0.9 V, I = 0.2 nA) and Sn-down (2.0 × 2.0 nm^2, V_{sample} = −1.8 V, I = 0.2 nA) molecules adsorbed on a single SnPc layer. The single arrow between (c) and (d) illustrates the irreversible switching from Sn-up to Sn-down conformations, while the double arrow between (e) and (f) illustrates the reversible switching. Reprinted from ref. 56, with permission from the American Chemical Society, copyright 2009.

irreversibly from the Sn-up to the Sn-down conformation by applying a negative sample voltage (Fig. 7c and d). The reversible

Open Access Article. Published on 11 March 2015. Downloaded on 6/24/2024 3:25:25 PM.
This article is licensed under a Creative Commons Attribution 3.0 Unported Licence.

switching between Sn-up and Sn-down can only be achieved on the second layer SnPc, as shown in Fig. 7e and f. From their experimental observations and calculations, they proposed that the transition from Sn-up to Sn-down is achieved *via* hole attachment. The resonant tunneling out of the highest occupied molecular orbital (HOMO) − 1 of Sn^{2+} creates a transiently oxidized Sn^{3+}, which is smaller than Sn^{2+}. The applied pulse voltage provides energy to move the Sn^{3+} further towards the substrate surface. The most likely mechanism leading to the Sn-down to Sn-up switching is the excitation of intramolecular vibrations. This switching is induced by the positive sample bias. The resonant transfer of tunneling electrons to the lowest unoccupied molecular orbital (LUMO) + 1 gives rise to a negatively charged and thus transiently reduced molecule. Upon leaving the molecule, the electrons may deposit energy to vibrational degrees of freedom of the molecule and thus excite the switching process.

Reversible switching of a single-dipole molecule of chloroaluminium phthalocyanine (ClAlPc) in an ordered molecular array on graphite has also been demonstrated by Huang *et al.*[98] The operating mechanism is based on reversible dipole switching. As the nonplanar dipolar molecule possesses an out-of-plane electric dipole moment of 3.7 D, it adopts two distinct configurations on graphite, namely, Cl-up and Cl-down. Fig. 8a shows the optimized ClAlPc molecular structure based on DFT

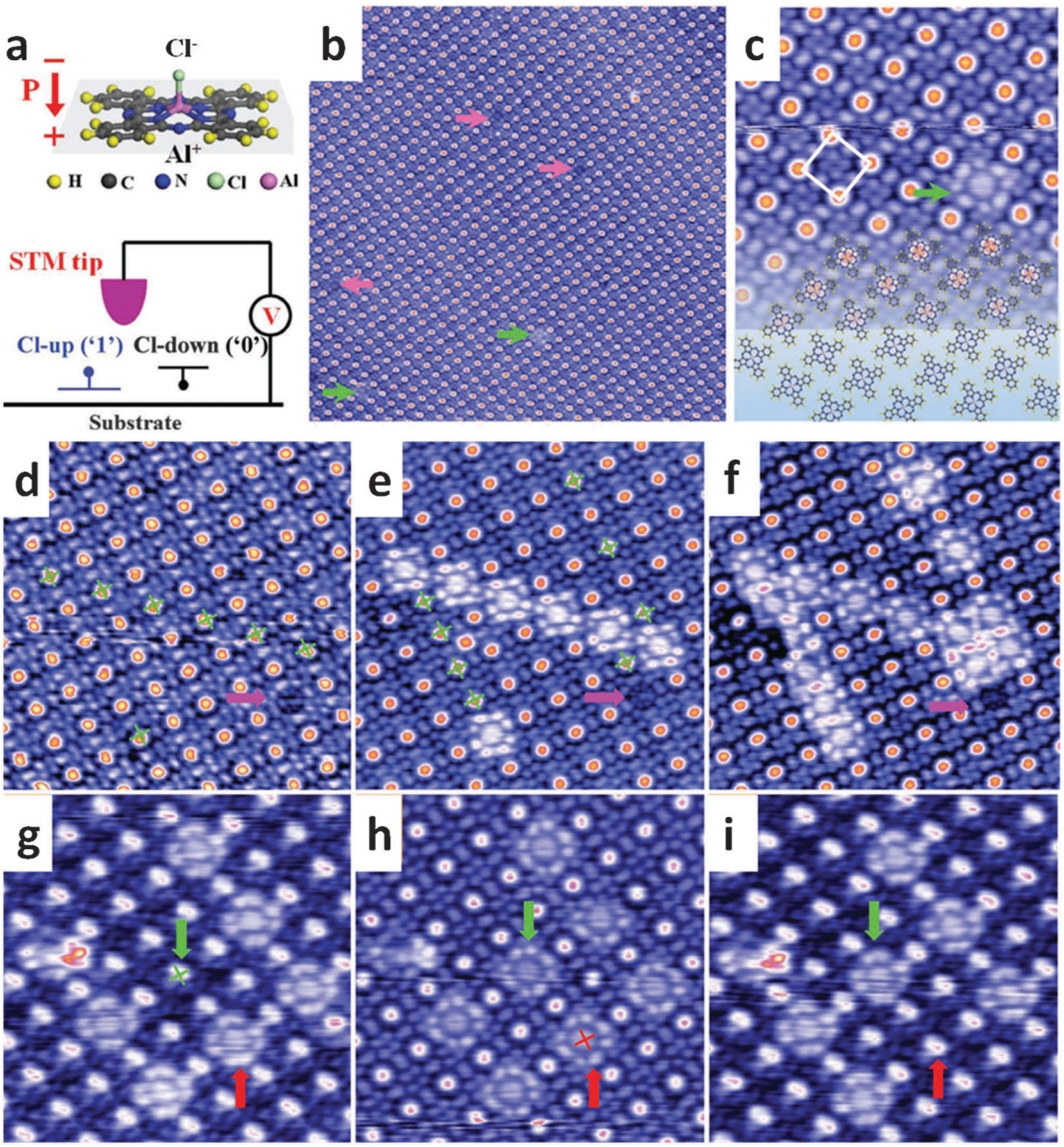

Fig. 8 (a) A schematic drawing shows the chemical structure of the ClAlPc molecule, the nonplanar molecule can adopt Cl-up and Cl-down configuration on a surface. (b) Large scale STM image demonstrates the formation of the molecular dipole monolayer by aligning the ClAlPc molecules in Cl-up configuration (V_{tip} = 2.5 V; 50 × 50 nm^2; 77 K). (c) The sub-molecularly resolved STM image (V_{tip} = 2.0 V; 10 × 10 nm^2; 77 K). (d–f) A letter 'N' was recorded by applying a series of voltage pulses (V_{tip} = 2.2 V; 12 × 12 nm^2; 5 K). (g–i) Images demonstrating the process of transforming the 'U' pattern to an 'H' pattern (V_{tip} = 2.5 V; 10 × 10 nm^2; 5 K). Green crosses denote the target molecules where positive voltage pulses (+4.5 V, 2 ms) were applied, and the red crosses indicate where negative pulses (−3 V, 2 ms) were applied. Reprinted from ref. 98, with permission from Wiley-VCH Verlag GmbH, copyright 2012.

Open Access Article. Published on 11 March 2015. Downloaded on 6/24/2024 3:25:25 PM.
This article is licensed under a Creative Commons Attribution 3.0 Unported Licence.

calculation. When adsorbed on the graphite surface, the ClAlPc molecules are spontaneously aligned in the Cl-up configuration, forming a highly-ordered close-packed structure (Fig. 8b) stabilized by interfacial π–π interactions. Each molecule appears as a four-lobe feature with a central protrusion (corresponding to the Cl-up configuration, Fig. 8c).

Single molecule switching can be realized in this monolayer by positioning the STM tip above the target molecule and subsequently applying a voltage pulse. A letter 'N' is successfully written in the molecular dipole array at 5 K, by applying a series of positive voltage pulses of +4.5 V for 2 ms. The molecules marked by the green crosses are switched from the Cl-up to the Cl-down configuration after pulsing (Fig. 8d–f). Letters 'U' and 'H' are written sequentially through the similar processes (Fig. 8g–i). The reversible switching from the Cl-down to the Cl-up configuration is realized with a negative bias voltage. As demonstrated in Fig. 8h and i, the Cl-down molecule denoted by the red cross in Fig. 8h is pulsed by a negative voltage of (−3 V, 2 ms) and it switches back to the Cl-up configuration (Fig. 8i).

Incorporation of these dipole molecular switches into two-dimensional hydrogen bonded binary molecular networks formed by perfluoropentacene (PFP) and ClAlPc has also been demonstrated.[97] By varying the binary molecular ratio, the interdipole separation in the molecular dipole dot arrays and hence the dipole densities can be easily tuned with molecular precision.

Moreover, formation of multiple intermolecular hydrogen bonds between the periphery F atom on PFP and the H atom of neighboring ClAlPc molecules can further enhance the structure stability during the switching. Fig. 9a shows a highly ordered "square" network formed by PFP and ClAlPc with a binary molecular ratio of 2 : 1. High-resolution STM images (Fig. 9b and c) reveals that all ClAlPc molecules are well separated by neighboring PFP molecules, which enables independent addressing at the single-molecule scale.

Switching between the Cl-up and the Cl-down can also be realized in this "square" network, as shown in Fig. 9e–h. The molecule indicated by the yellow circle can be switched from the Cl-up (Fig. 9e) to the Cl-down configuration (Fig. 9f) by

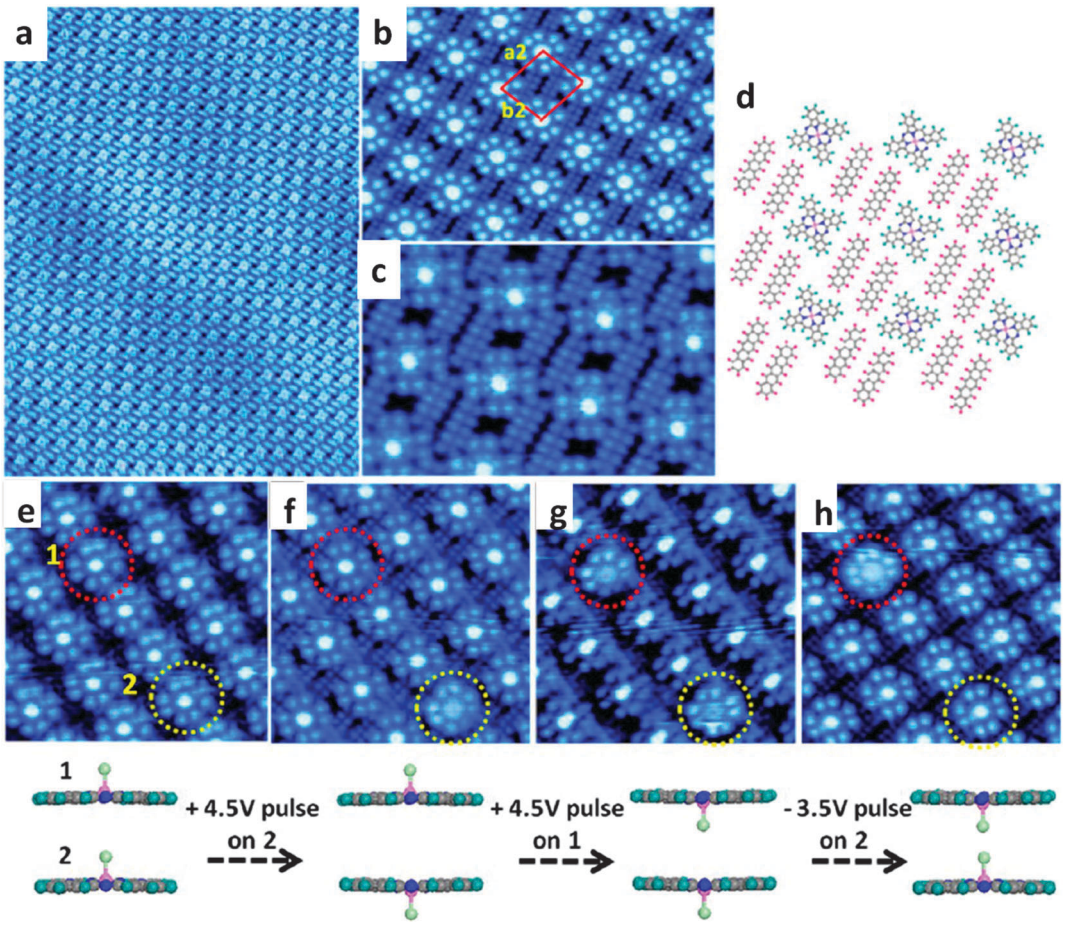

Fig. 9 (a) STM image (V_{tip} = 2.0 V; 45 × 60 nm^2; 77 K) of a long-range-ordered "square" binary molecular network formed by PFP and ClAlPc with a binary molecular ratio of 2 : 1 on HOPG. (b) High-resolution STM images of the "square" structure: (V_{tip} = 2.5 V; 15 × 10 nm^2; 77 K) and (c) (V_{tip} = 2.0 V; 9 × 6 nm^2; 77 K). (d) Schematic packing structure for the "square" network. (e–h) Sequential STM images showing the reversible switching between the Cl-up and the Cl-down configurations (V_{tip} = 2.1, 2.0, 2.0, 2.2 V; 10 × 10 nm^2; 77 K). Molecule indicate by the red circle (molecule 1) was switched from Cl-up (b) to Cl-down (c) by a positive voltage (+4.5 V, 5 ms), and molecule indicated by the yellow circle (molecule 2) was switched from the Cl-up configuration (a) to the Cl-down configuration (b) by a positive voltage pulse and back to the Cl-up configuration (d) by applying a negative pulse (−3.5 V, 5 ms). Corresponding schematics demonstrating the switching of molecules 1 and 2 are shown below each STM image. Reprinted from ref. 97, with permission from the American Chemical Society, copyright 2014.

 This journal is © The Royal Society of Chemistry 2015

Open Access Article. Published on 11 March 2015. Downloaded on 6/24/2024 3:25:25 PM.
This article is licensed under a Creative Commons Attribution 3.0 Unported Licence.

applying a positive voltage pulse of 4.5 V for 5 ms, and then back to the Cl-up configuration (Fig. 9h) by applying a negative voltage pulse of −3.5 V for 5 ms. It is worth noting that only one ClAlPc molecule directly under the STM tip is switched with the neighboring hydrogen bonded molecular networks unaffected, and the in-plane orientation of the switched molecule unchanged. It is proposed that the reversible switching is induced by the "shuttling" of the Cl atom between two sides of the ClAlPc molecular plane. The nudged elastic band (NBE) algorithm was employed to reveal the minimum-energy pathway for Cl-atom shuttling. The energy barrier for a single switching process is found to be 2.89 eV for the minimum-energy path, which is in close agreement with the experimentally observed threshold voltage. Such reversible and controllable dipole switching is spatially confined to the addressed molecule, and leaves the neighboring binary molecular network unaffected, demonstrating its potential in high-density data storage molecular devices.

3.3 Spin switching

The emerging field of molecular spintronics combines the ideas and advantages of spintronics and molecular electronics.[47] A fundamental link between these two fields can be established by using molecular magnetic materials, in particular, single-molecule magnets (SMM).[41,100,153] SMM have been investigated for their rich quantum behavior, such as quantum tunneling of magnetization,[154] quantum phase interference,[155] the Kondo effect[23] and Zeeman splitting of the Coulomb-blockade peaks.[156] Due to the presence of large spin and high anisotropy barrier, SMM in a time-dependent magnetic field exhibits magnetic hysteresis loops.[157] This presents an exciting opportunity perspective of exploiting spins to store and process information.

Using the double-decker bis(phthalocyaninato) terbium(III) complex ($TbPc_2$) as a SMM,[158] Komeda *et al.* showed that the molecular spin can be switched on and off by applying an electric current *via* an STM.[146] The switching is manifested through the disappearance and reappearance of the Kondo resonance. The Kondo effect arises from the coupling between a localized electron spin and a sea of conduction electrons.[159–161] Fig. 10a shows an STM image of an isolated $TbPc_2$ adsorbed on Au(111). Fig. 10b and c are the schematic models of the top view and side view of $TbPc_2$. Two Pc ligands sandwich a Tb ion with an azimuthal rotational angle of 45°. A simulated STM image of the $TbPc_2$ molecule on Au(111) is shown in Fig. 10d, and indicates that the eight protrusions in the STM images are from the upper Pc ligand. $TbPc_2$ in a monolayer film forms a

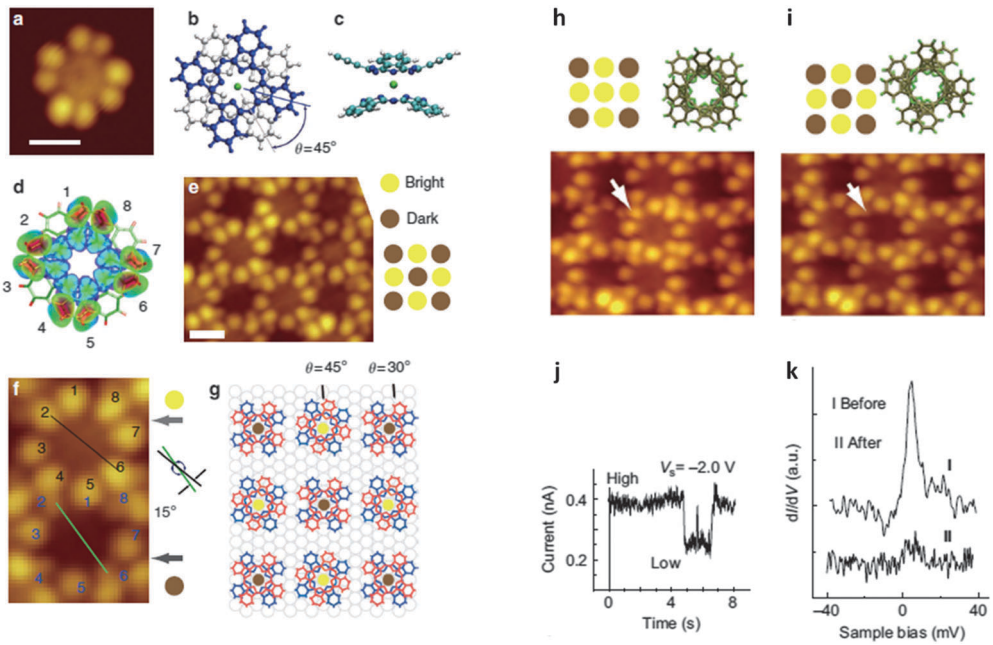

Fig. 10 (a) STM image of an isolated molecule of $TbPc_2$ on Au(111). (b) A schematic model of the double-decker $TbPc_2$ molecule. The upper (lower) Pc is coloured in blue (silver). (c) Side view of the $TbPc_2$ molecule after structural optimization by using DFT calculations. (d) A simulated STM image of the $TbPc_2$ molecule by DFT calculations. (e) Film of $TbPc_2$. An alternating contrast pattern of nine molecules is shown on the right hand side with brighter molecules in yellow and darker molecules in brown. (STM images of a and e were obtained with V_{sample} = −0.8 V and I = 0.3 nA. Bars correspond to 1 nm). (f) A magnified image of bright (upper) and dark (lower) molecules. The black (green) line connects lobes 2 and 6 of bright and dark molecules. The two lines are rotated 15° with respect to each other. (g) A tentative model of the adsorption configuration of the $TbPc_2$ film, corresponding to the image in e. Bright (θ = 45°) and dark (θ = 30°) molecules form a pseudo-square lattice, and the red and blue Pc ligands correspond to vacuum- and substrate-side Pc ligands, respectively. (h) and (i) conversion of the centre molecule from bright (θ = 45°) to dark (θ = 30°) by applying a current pulse. The target molecule is marked by an arrow. Change in the contrast and the top view of the centre molecule are schematically illustrated. (j) Current during a −2.0 V voltage pluse over a $TbPc_2$ molecule initially in the bright state. The tip remained fixed over a lobe position with the feedback loop open. Each jump in the current indicates the moment of rotation of the molecule and low state corresponds to the dark state. (k) Comparison of the Kondo peaks before I and after II the application of the pulse. Reprinted from ref. 146, with permission from Nature Publishing Group, copyright 2011.

Open Access Article. Published on 11 March 2015. Downloaded on 6/24/2024 3:25:25 PM.
This article is licensed under a Creative Commons Attribution 3.0 Unported Licence.

checkerboard contrast pattern, as depicted on the right hand side of Fig. 10e. The bright and dark molecules are shown in yellow and brown colors, respectively. The magnified image in Fig. 10f reveals that the upper Pc ligand of the bright and dark molecules are rotated 15° with respect to each other. The bright and dark molecules can be switched between each state by injecting enough current *via* the STM tip. As shown in Fig. 10h and i, the centre molecule is converted from bright to dark by applying a pulse V_{sample} to the molecule. Rotation of a molecule can be monitored by the tunneling current change, as shown in Fig. 10j. The high and low states of the tunneling current correspond to the bright and dark state respectively. The log–log plot of the rotation rate *versus* tunneling current yields a slope of ~1.09. This suggests that the current-induced rotation is a one-electron process. Fig. 10k shows the analysis of tunneling conductance (dI/dV) on a $TbPc_2$ molecule. A clear Kondo resonance is observed when the tip is positioned over one of the lobes of the bright molecule. However, the Kondo feature disappears for the dark molecule. Moreover, when the tip is placed over the center of the bright or dark molecule, no Kondo feature can be observed. This indicates that an unpaired electron in a π orbital of the upper Pc ligand of the bright molecule is responsible for the appearance of the Kondo peak. DFT calculations shows that upon rotation of the upper Pc ligand by 45°, the singly occupied molecular orbital (SOMO) moved toward the Fermi energy. Hence, in the presence of the Au(111) surface, the SOMO became doubly occupied near θ = 30° due to charge transfer from the surface, quenching the molecular spin and the Kondo state. The controlled on and off switching of a molecular spin makes it possible to code information at the single-molecule level.

3.4 Charge switching

Molecular charge switching requires bistability of the charge states of the molecule. This can be achieved if (i) the lifetime of the tunneling electron on the molecule is sufficiently long and (ii) there is a mechanism that stabilizes the extra charge on the molecule.[63,82,162] If the atom/molecule is directly adsorbed on a metal surface, the strong coupling between them can neutralize the charge residing on the atom/molecule. However, if the atom/molecule is adsorbed on an ultrathin insulating film, the life time of the electron on the atom/molecule can be considerably increased, leading to a stable charge state.

Repp *et al.* showed that individual gold atoms on an ultrathin insulating NaCl film supported by a copper surface can exhibit two different charge states.[63] As shown in Fig. 11a, individual Au atoms on NaCl(100)/Cu(111) are imaged as protrusions. By applying a positive 0.6 V to the sample and monitoring the current, a sharp decrease in the tunneling current can be observed (Fig. 11d). The subsequent STM image in Fig. 11b shows that the manipulated Au adatom now has a sombrero-like shape. By applying a negative voltage pulse to the sample, the Au adatom can be switched back to its original state, as shown in Fig. 11c. The two states before and after manipulation are assigned to the neutral and negatively charged states, respectively, as further confirmed by DFT calculations. As shown in Fig. 11e–j, for the Au^0 adatom, a weak bond is formed with a binding energy of 0.4 eV. It is

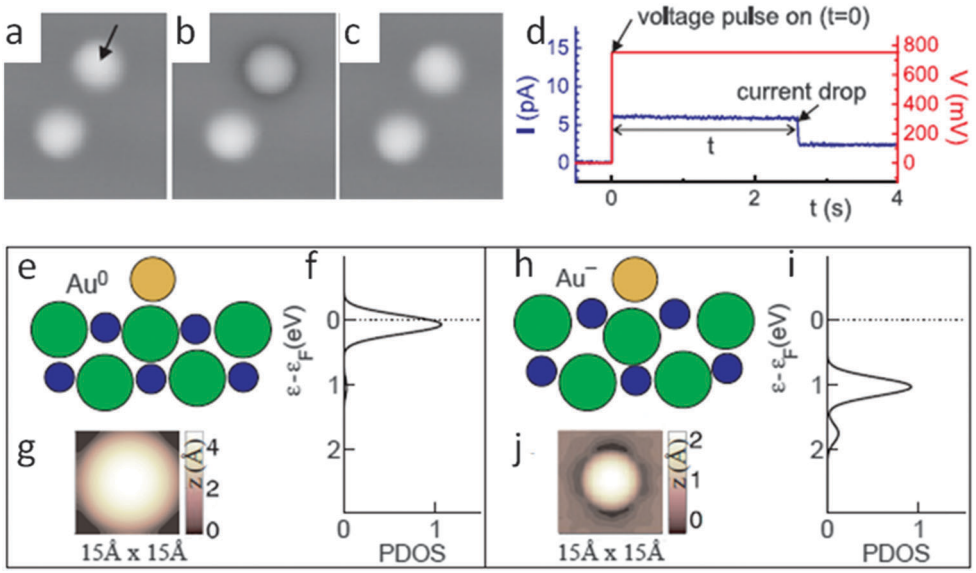

Fig. 11 (a) STM image of Au adatom on NaCl/Cu(111). After recording the image (a), the STM tip was positioned above one of the Au adatom (arrow) and a positive voltage pluse was applied to the sample. After a time *t*, a sharp decrease in the tunneling current can be observed in (d). A subsequent STM image (b) shows that the manipulated Au adatom has a different appearance but did not change its position. By applying a negatibe voltage pulse, one can switch the manipulated adatom back to its initial state (c). (e)–(g) Calculated electronic and geometric properties of the neutral and (h)–(j) negatively charged Au adatom. The ion-core positions are represented by a sphere model (e and h), in which the spheres representing Au, Cl^-, and Na^+ are clolored gold, green, and blue, respectively. The calculated partial density of states (PDOS) of s-states at the Au adatom (f and i). the 6s-derived state is partially and fully occupied in (f) and (j). STM images are simulated by contours of constant LDOS (g and j), where z = 0 Å corresponds to a distance of 6.4 Å from the topmost NaCl reference plane. Reprinted from ref. 63, with permission from the American Association for the Advancement of Science, copyright 2004.

Open Access Article. Published on 11 March 2015. Downloaded on 6/24/2024 3:25:25 PM.
This article is licensed under a Creative Commons Attribution 3.0 Unported Licence.

adsorbed about 3.2 Å above the Cl^- ion and leaves the ionic positions within the NaCl film relatively unperturbed. However, the position of the Au^- adatom is 0.4 Å closer to the surface, and is stabilized by large ionic relaxations within the NaCl film. The Cl^- ion underneath the adatom is forced to move downward by 0.6 Å, and the surrounding Na^+ ions move upward by 0.6 Å. This relaxation pattern creates an attractive potential for the additional charge on the Au adatom. The additional charge is further stabilized by the screening charge in the metal substrate and by the electronic polarization of the ionic layer. Statistical analysis of the switching behavior of Au adatoms suggests that the switching between two charge states is attributed to inelastic electron tunneling.

3.5 Bonding switching

Due to its ability to image and manipulate adsorbates at the atomic scale, the STM is also a powerful tool for molecular-scale chemical reaction studies, such as dissociation, diffusion, adsorption, desorption and bond-formation processes.[86] Complex mechanisms are involved when forming a bond between two adsorbed molecular fragments on a surface. To form a bond between them, the electronic wave functions of their reactive parts need to overlap significantly. Hence, they have to be in close proximity on the surface and their reactive parts must align properly. Mohn *et al.* have presented a molecular switch based on the reversible bond formation between a Au adatom and an organic admolecule [perylene-3,4,9,10-tetracarboxylic dianhydride (PTCDA)] on a thin NaCl film supported by a Cu substrate.[62]

The reversible switching of a Au–PTCDA complex on NaCl(2 ML)/Cu(111) is shown in Fig. 12a–c. Initially, a Au^- adatom is brought in close proximity to a $PTCDA^-$ adamolecule (Fig. 12a). Then the sample bias is ramped to −1.5 V. The subsequent STM image shows that the complex has been switched to a different state (Fig. 12b). By ramping the bias voltage to +1.5 V, the complex can be switched back to the initial state (Fig. 12c). The different states of the complex are assigned to the nonbonded [Au–PTCDA(N)] and bonded [Au–PTCDA(B)]. To determine the atomic structure of the different configurations of Au–PTCDA, atomically resolved atomic force microscopy (AFM) molecular imaging is used. As shown in Fig. 12g–i, the perylene core of PTCDA is clearly resolved in the AFM images. For Au–PTCDA(N), the AFM image shows that the molecule and the Au adatom are clearly separated. In contrast, for the Au–PTCDA(B), the Au atom is no longer separated from the molecule and the brightness of the lower part of the atom-molecule complex is enhanced. A distinct enhancement of the brightness is observed above one of the two inner C sites at the lower edge of the molecule, and the two mirrored configurations are clearly distinguished. The experimental results are corroborated by DFT calculations, as shown in the calculated atomic structures of the complex in Fig. 12j and k. A more detailed calculation of the partial density of states (PDOS) reveals that a covalent bond is formed between the Au adatom and PTCDA for Au–PTCDA(B).

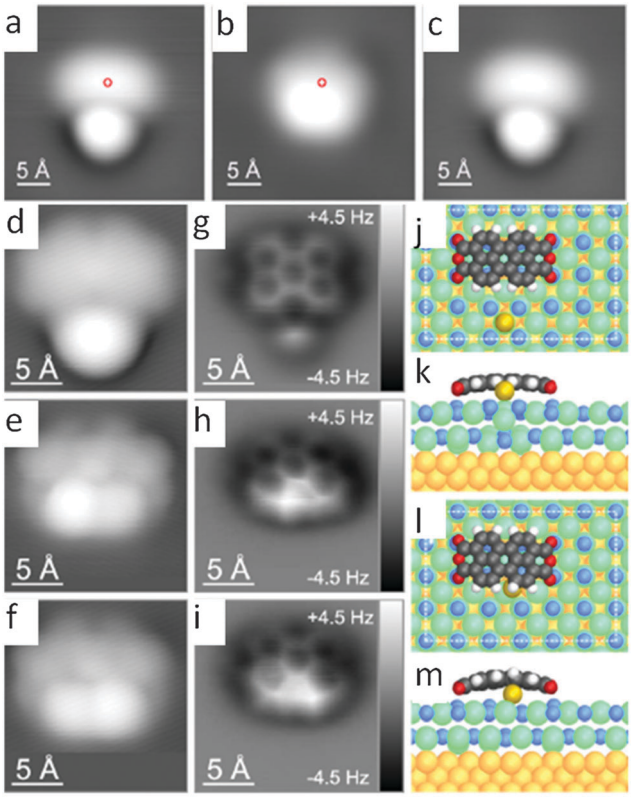

Fig. 12 (a) Au-adatom in close proximity of a Au–PTCDA complex. With the tip at the position indicated by the (red) circle, the sample bias voltage V was ramped to −1.5 V. A sudden increase in the tunneling current I indicated a successful modification of the complex. (b) In the subsequent STM image, the adatom and the molecule no longer appeared separated. By ramping the voltage to +1.5 V, the complex was switched back to the initial state, as confirmed by the subsequent image (c). Imaging parameters: V_{sample} = 0.2 V, I = 5 pA. (d)–(f) STM images of Au–PTCDA in the nonbonded (a) and the bonded [(b), (c)] configuration (imaging parameters: V_{sample} = 0.2 V, I = 3 pA). The tip had been terminated with a CO molecule. (g)–(i) Corresponding constant-height AFM images (imaging parameter: amplitude A = 0.4 Å, frequency f = 23, 165 Hz and distance with respect to the STM set point above the substrate between +0.8 Å and +1.0 Å). (j)–(m) DFT-calculated geometries of the complex in the nonbonded [(j), (k)] and the bonded [(l), (m)] state. The unit cell used for the calculations is indicated in (j) and (l), and the different atomic species are colored in gray (C), red (O), white (H), green (Cl), blue (Na), orange (Cu), and yellow (Au). Reprinted from ref. 62, with permission from the American Physical Society, copyright 2010.

4. Conductance switching

The single molecule switches can also be realized for the functional molecules covalently bonded with the electrode. These configurations can be formed by depositing self-assembled monolayers (SAMs) of amphifunctional molecules on surfaces. The amphifunctional molecules usually have one end with strong affinity that can chemically bond to the surface and another end that has weak affinity or none. There are several types of SAMs with the elegant examples including organosilicon on hydroxylated surfaces, alkanethiolates on gold, silver and copper, alcohols and amines on platinum, and carboxylic acids on aluminum oxide, silver oxide and glass.[163–166] Among them, the conductivity

Open Access Article. Published on 11 March 2015. Downloaded on 6/24/2024 3:25:25 PM.
This article is licensed under a Creative Commons Attribution 3.0 Unported Licence.

of the thio-terminated conjugated molecules such as polythiophenes, polyphenylenes, polyanalines, polyphenylenevinylenes, and oligo(phenylene-ethynylene)s (OPEs) are widely investigated.[64,167–173] The initial goal of the previous study was to investigate their potential use as molecular wires.[5,174,175] Following works have shown that they also exhibit other interesting electronic characteristics, for example, negative differential resistance (NDR)[176,177] and bistable switching.[64,171]

The bistable conductance switching of the OPE molecules have been extensively studied both theoretically and experimentally.[64,167,171,178–185] Donhauser *et al.* have demonstrated the conductance switching of single and bundled OPE molecules isolated in matrix of alkanethiolate monolayers.[64] Fig. 13a shows the molecular structures for the investigated OPE molecules. Aqueous ammonium hydroxide is used to hydrolyze the acetyl protecting group, generating a thiolate or thiol. These thiolate/thiol molecules can then adsorb on Au(111), inserting at the defect sites such as substrate step edges, film domain boundaries and vacancies on the alkanethiolate monolayer. At these sites, the gold surface is exposed and hence the sulfur head groups can chemisorb to the gold surface and the conjugated tails can protrude from the film. Fig. 13b shows STM image of a single 3′ molecule isolated in a dodecanethiolate monolayer matrix. A high-resolution image in Fig. 13c reveals that molecule 3′ is adsorbed in the domain boundary. During the continued STM scanning, this molecule can change from the high conductance state (“on” state) to the low conductance state (“off” state), as shown in Fig. 13d and e. Similar conductance switching can also be observed for molecules 2′ and 3′. Fig. 13f shows a time-lapse series of images of molecule 2′ recorded over several hours. Reversible switching between “on” and “off” states occurs several times in the first 50 frames, and then the molecule stabilizes in the “on” state for the remaining images. It is found that the well ordered surrounding matrix can result in low switching rate; while a poorly ordered matrix increases the switching rate. As the poorly ordered films have higher degrees of conformational relaxation and allow more freedom of the movement for the isolated molecule, it is proposed that the switching results from the conformational changes of the imbedded molecule. Different mechanisms in the conductance switching are also proposed by other groups, including reduction of the functional group,[178] rotation of the functional group,[179] rotation of the conjugated backbone,[180] intermolecular interactions,[181] bond fluctuations[171] and changes in hybridization of metal-molecule bonds.[64,167,183,184]

In order to find out the mechanism that is most responsible for the conductance switching, Moore *et al.* tested each hypothesized mechanism through the engineering of the molecular structure.[186] Fig. 14 shows the conjugated molecules that they used to test the proposed mechanisms. The theoretical study of Seminario *et al.* suggested that the conduction of a nitro- and amino-functionalized molecule is through the

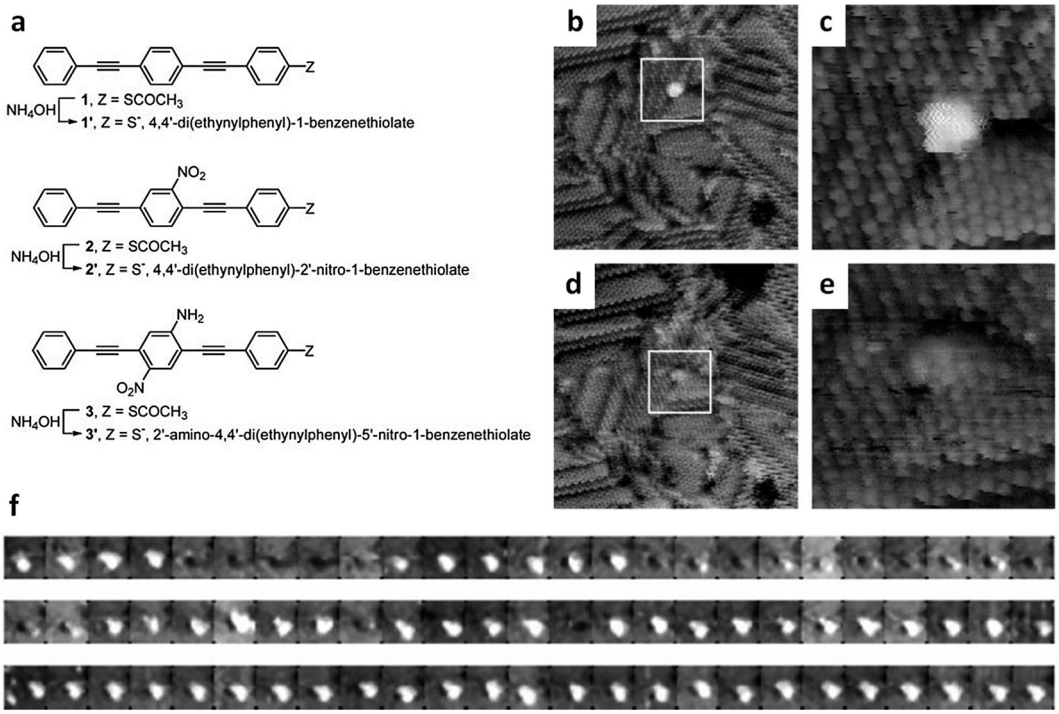

Fig. 13 (a) Molecular structures of the investigated molecules. Aqueous ammonia hydroxide is used to hydrolyze the acetyl protecting group, generating the thiolate or thiol. (b) Topographic STM image of a molecular switch 3′ inserted in a dodecanethiol SAM. A molecule of 3′ is highlighted by the square (20 × 20 nm^2). (c) A high-resolution STM image (5 × 5 nm^2) of the same area. The molecule is adsorbed in the domain boundary that separates the tightly packed dodecanethiol domains in the lower right and upper left areas of the images. (d) STM image of the same molecule 3′ in the off state (20 × 20 nm^2). (e) A high-resolution STM image of the same area in panel d (5 × 5 nm^2). (f) A time-lapse series of images of molecule 2′ acquired over several hours. The time interval between frames is ~6 min. Reprinted from ref. 64, with permission from The American Association for the Advancement of Science, copyright 2001.

Open Access Article. Published on 11 March 2015. Downloaded on 6/24/2024 3:25:25 PM.
This article is licensed under a Creative Commons Attribution 3.0 Unported Licence.

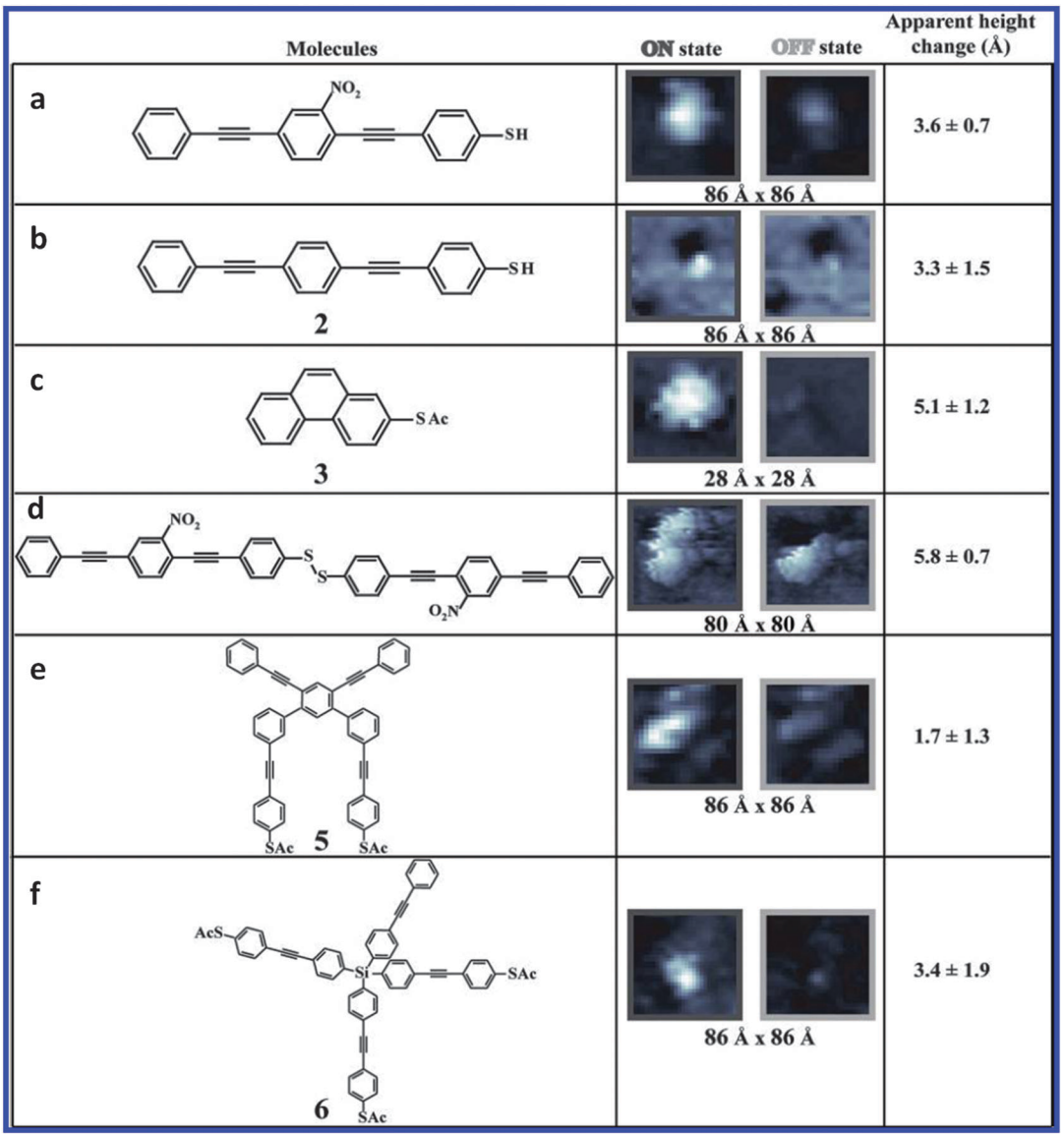

Fig. 14 Molecular structures, extracted images of molecules isolated in alkanethiolate SAMs in both ''on'' and ''off'' conductance states, and the average measured differences in apparent heights between states (matrix dependent) for each type of inserted molecule. (a) Nitro-functionalized OPE molecule 1 in a decanethiolate SAM, V_{sample} = −1 V, I_{tunnel} = 2 pA. (b) Unfunctionalized OPE molecule 2 in a decanethiolated SAM, V_{sample} = −1 V, I_{tunnel} = 2 pA. (c) Phenanthrene-based molecule 3 in an octanethiolate SAM, V_{sample} = −1 V, I_{tunnel} = 3 pA. (d) Disulfide OPE molecule 4 prepared by oxidative homocoupling of the thiol from 1 in an octanethiolate SAM, V_{sample} = −1 V, I_{tunnel} = 2 pA. (e) Two-contact OPE molecule 5 in a dodecanethiolate SAM V_{sample} = −1 V, I_{tunnel} = 1 pA. (f) Caltrop molecule in a dodecanethiolate SAM, V_{sample} = −1 V, I_{tunnel} = 1 pA. Reprinted from ref. 186, with permission from American Chemical Society, copyright 2006.

LUMO, thus the conduction depends on the LUMO spatial extent and the HOMO–LUMO gap.[178] The neutral molecule is an insulator due to the localization of the LUMO. However, once it is reduced by an applied bias larger than 1.74 V, the molecule becomes charged by one electron and the LUMO extends over the whole molecule. In this case, the conductance switching is a result of the reduction of the functional group. However, Moore observed the conductance switching at ±1 V sample bias, which is smaller than the threshold reducing potential (1.74 V). Moreover, the unfunctionalized molecule 2 (Fig. 14b) exhibits the same stochastic conductance switching. This suggests that the conductance switching is not due to the functional group reduction. The first principle calculations by Ventra *et al.* suggested that the rotation of the ligand functional group can modify the transport properties of single molecules.[179] As this mechanism requires the attachment of substituent groups on the conjugated molecule, hence it is also excluded by the observation of conductance switching for the unfunctionalized OPE molecule. Cornil *et al.* proposed that the conductance can be modulated by the rotation of the conjugated backbone.[180] To test this mechanism, the phenanthrene molecule 3 was synthesized. In this molecule, the aromatic rings are fused into a same molecular plane and hence preclude the rotation of the phenyl ring. However, the conductance

Open Access Article. Published on 11 March 2015. Downloaded on 6/24/2024 3:25:25 PM.
This article is licensed under a Creative Commons Attribution 3.0 Unported Licence.

switching between two states is observed for molecule 3. This indicates that the rotation of the conjugated backbone is not the origin of the conductance switching. It is also proposed that the varied interactions with neighboring molecules can also cause the conductance switching. Theoretical studies of Lang *et al.* suggested a reduction of the conductance for a pair of "carbon wires" at low bias connected in parallel compared to a single isolated wire.[181] To test this mechanism, disulfide forms of nitro-functionalized OPE molecules 4 were synthesized and inserted into the host matrix. Disulfide molecules dissociatively chemisorb with the sulfur atom bond to Au(111). Fig. 14d shows the conductance switching for one inserted pair. The upper molecule exhibits conductance switching from the "on" state to the "off" state; while the lower molecule remains in the "on" state. No significant difference in conductance is observed for the molecules existing in pairs or as a single molecule, thus eliminating the intermolecular interactions as the origin for the conductance switching. By using a top gold contact configuration, Ramachandran *et al.* argued that the conductance switching is caused by the "blinking" of a thiol–gold bond.[171] However, they cannot exclude the possibility that the "on/off" switching observed in their experiment is caused by the fluctuations of the nonbonded top contact, where the gold particles are swept away during the scanning. Weiss *et al.* suggested that a change in the hybridization between the conjugated molecules and substrate causes the conductance switching.[64,167] The hybridization change can occur through a change in the alignment with the surface. Sellers *et al.* suggest that the S–Au can have a sp hybridization with the molecule oriented normal to the surface, or sp^3 hybridization with a tilted conformation.[183,184] The common feature of the investigated molecules in Fig. 14 is that they all possess the S–Au bonding. If the change in the bond hybridization leads to the conductance switching, the host films must have enough free space to allow the tilt of the molecule. This is consistent with the observation that the closed packed SAMs result in a low switching rate while the poorly ordered SAMs lead to high switching rate. This mechanism is further confirmed by the bias-dependent conductance switching of OPE molecules with dipole moments.[169] The electrostatic attraction or repulsion between the STM tip and the dipole moment of the OPE molecules can cause the molecule to adopt standup or tilt configuration. In this case, the conductance switching of the molecule can be controlled by an applied electric field.

In the conductance switching experiment described above, the molecule is covalently bonded to one electrode (*i.e.*, the substrate), with the other end probed by the STM tip with a tunneling gap in between. It is also possible for the molecule to bond covalently to both electrodes. This is the break junction configuration that will be discussed in the next section.

5. Single molecule switches developed using single molecule junctions

In addition to switches formed on surfaces investigated by STM, single molecule switches have also been intensively investigated using single molecule junctions,[187] for example, scanning probe microscopy (SPM) based break junctions,[9,11,12,21,188–192] mechanically controlled break junction (MCBJs)[5,22,193–201] and electromigration break junctions (EBJs).[23,156,202–209] The advantage of SPM-based break junction is that it allows the direct visualization of the molecular junction and the simultaneous charge transport measurement. A metal-molecule-metal junction between the metallic tip and the substrate containing the molecules can be formed by repeatedly crashing the tip into and out of contact with the substrate.[6,8,9,18,182–186] A schematic illustration of the STM-based break junction is shown in Fig. 15a. Fig. 15b shows the layout of the MCBJs set-up, a metallic wire fixed on a flexible substrate starts to elongate and finally fractures by the vertical movement of the piezo-controlled push rod. Electrodes with a gap of sub-angstrom precision can be fabricated using this method. By using MCBJs, a metal–molecule–metal junction can be repeatedly formed and broken and the gap size can be precisely and continuously adjusted.[5,22,193–201] This enables collecting statistical data for the metal/molecule interfaces with different geometry structures. Electromigration has also been utilized to fabricate nanogap electrodes for single molecule junctions.[20,151,196–203] Applying a large current to a thin metal wire causes the migration of the metal atoms and results in the breakage of the nanowire with the formation 1–2 nm gap. The EBJs method facilitates the ease of the fabrication of three-terminal devices

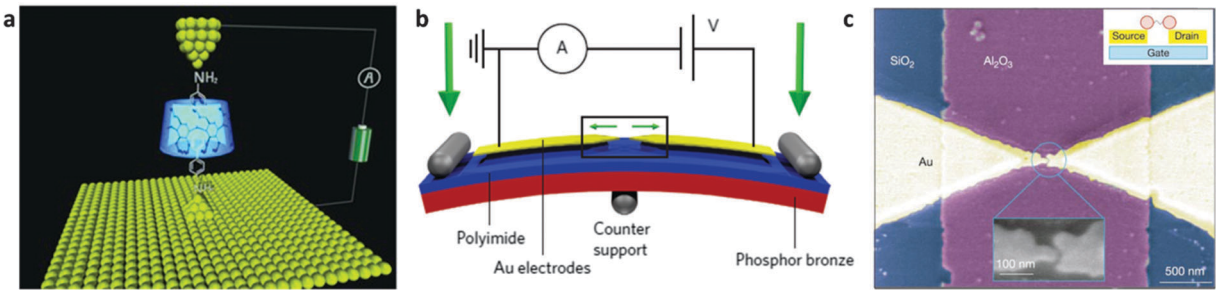

Fig. 15 (a) Schematic illustration of the STM-based break junction.[21] (b) Layout of the MCBJ set-up.[22] (c) A single electron transistor fabricated using the EBJ method.[23] (a) Reprinted from ref. 21, with permission from John Wiley and Sons, copyright 2012. (b) Reprinted from ref. 22, with permission from Nature Publishing Group, copyright 2013. (c) Reprinted from ref. 23, with permission from Nature Publishing Group, copyright 2002.

 This journal is © The Royal Society of Chemistry 2015

Open Access Article. Published on 11 March 2015. Downloaded on 6/24/2024 3:25:25 PM.
This article is licensed under a Creative Commons Attribution 3.0 Unported Licence.

with the gate effect by forming the nanogap on top of an oxidized conducting substrate.[23,205,209]

Various single molecule switches have been demonstrated using these single molecule junctions, such as molecular isomerization,[201] spin switches,[195] field effect transistors[209] and diodes.[12] In this section, we will highlight the recent experimental work of these switches realized in single molecule junctions.

5.1 Molecular isomerization

During the past decades, extensive research efforts have been devoted to the understanding of the molecular conductance, ranging from isolated single molecule or self-assembled molecular networks on surfaces to single molecule junctions.[11,210] Molecules that can be reversibly switched between high and low conductance state represent the ideal building blocks for molecular electronics. A large proportion of the conductance switching is a result of the chemical bond switching of the molecule or a change in the contact configuration.[11,188,192,196,197,210,211]

Recently, Kim *et al.* demonstrated the molecular isomerization induced conductance switching of photochromic molecules using the MCBJs technique at low temperature.[201] Fig. 16a shows a SEM image of the single molecule device and a schematic illustration of a single diarylethene molecule bridged between two gold electrodes. The diarylethene molecules can be reversibly switched between open and closed forms as shown in Fig. 16b. The open isomer with a broken π-conjugation can switch to a closed form under UV light irradiation, which leads to a completely π-conjugated current path along the molecule. The reverse switching from close to open isomer can be triggered by the visible light irradiation. The closed isomer possesses a higher conductance than the open isomer due to its full π-conjugation along the current pathway. Fig. 16c shows the molecular structure of the four molecules investigated in this study. The typical conductance traces for the open and closed form for the four different molecules are displayed in Fig. 16d and e. The highest conductance plateau (G_0) in the figure corresponding to the single-atom Au–Au contact. Further stretching of the metallic bridge results in the trapping of the molecule in the junction and a sudden drop in the conductance is observed. Statistical data are collected by repeating this breaking and closing process about 1000 times for the open and closed form of each molecule. The lowest preferred conductance value corresponds to a single molecule junction. Fig. 16f–i show the measured *I–V* characteristics for the open and closed form of these four molecules in a single molecule junction. It is obvious that the closed form (CF) has a higher conductance than its corresponding open form (OF) for all these molecules. This indicates that the charge transport in the molecules is significantly influenced by the optically induced molecular isomerization.

5.2 Spin switching

Single molecule based spin switches can also be realized in the break junction configuration. Recently, Wagner *et al.* have demonstrated a bias induced spin switch of a single molecule between the pseudo-singlet state and the pseudo-triplet state using the MCBJs technique.[195] Fig. 17a shows the SEM image and the scheme of the break junction set-up. The molecular structure of the investigated molecule is shown in Fig. 17b. Two coupled spin centers are confined to two Co^{2+} ions and the magnetic coupling path is orthogonally orientated to the current pathway. Fig. 17d shows the temperature dependence of the differential conductance obtained for type I molecular junction. A zero bias anomaly (ZBA) with a Lorentzian shape is observed. The peak height G_{max} and peak width as a function of temperature are plotted in Fig. 17e and f. The conductance maximum increases logarithmically towards the low temperature while the peak width broadens towards the high temperature. These data fit well to the well-known Kondo behavior. The magnetic field dependence result reveals that the ZBA splits and moves outwards with increasing field, which further confirms its magnetic origin. Combined with the DFT calculations, the Kondo-like peak for the type I data is assigned to the pseudo-triplet state. Fig. 17g and j show the type I *I–V* characteristics and the corresponding differential conductance for several different samples. The type II *I–V* characteristics and the corresponding differential conductance are shown in Fig. 17h and k. A symmetric current step occurs for the type II data in the low bias regime at around ±0.2 V. This sudden transition is ascribed to the switch of the system. As no ZBA and no magnetic field response is observed in these curves, the inner part of the type II is assigned to the non-magnetic pseudo-single state of the molecule. The outer part in Fig. 17h is assigned to the pseudo-triplet state. A biastable state which includes type I and type II in a single curve have also been observed, as shown in Fig. 17i. This can give access to how the two types of data are related to one another and hence the switching in Fig. 17h can be interpreted as a transition from the non-magnetic pseudo-single state at low bias to the pseudo-triplet state at high bias. The underlying mechanism of this bias-induced switching is still unclear. The electric field-induced asymmetry is proposed as a driving force.

5.3 Field effect transistors

Building a single molecule field-effect transistor (FET) is considered as a critical step for the ultimate device miniaturization and integration of molecular electronic devices.[193,209] Tremendous challenges are met for the experimental demonstration of true three-terminal device, such as the reliable connection of a single molecule between the source and drain electrodes; precise placing of a gate electrode a few nanometers away from the molecule.[212] As mentioned above, the electromigration technique is an ideal method to fabricate three-terminal devices with gate effect by forming the nanogap on top of an oxidized conducting substrate.[23,205,209]

Song *et al.* have demonstrated the observation of a direct gate modulation of molecular orbitals.[209] They used electromigration to form electrode pairs with a nanometer-scale separation, which is placed over an oxidized aluminium gate electrode. The inset in Fig. 18a shows the device structure and the schematic of a single 1,8-octanedithiol (ODT) molecule in

Open Access Article. Published on 11 March 2015. Downloaded on 6/24/2024 3:25:25 PM.
This article is licensed under a Creative Commons Attribution 3.0 Unported Licence.

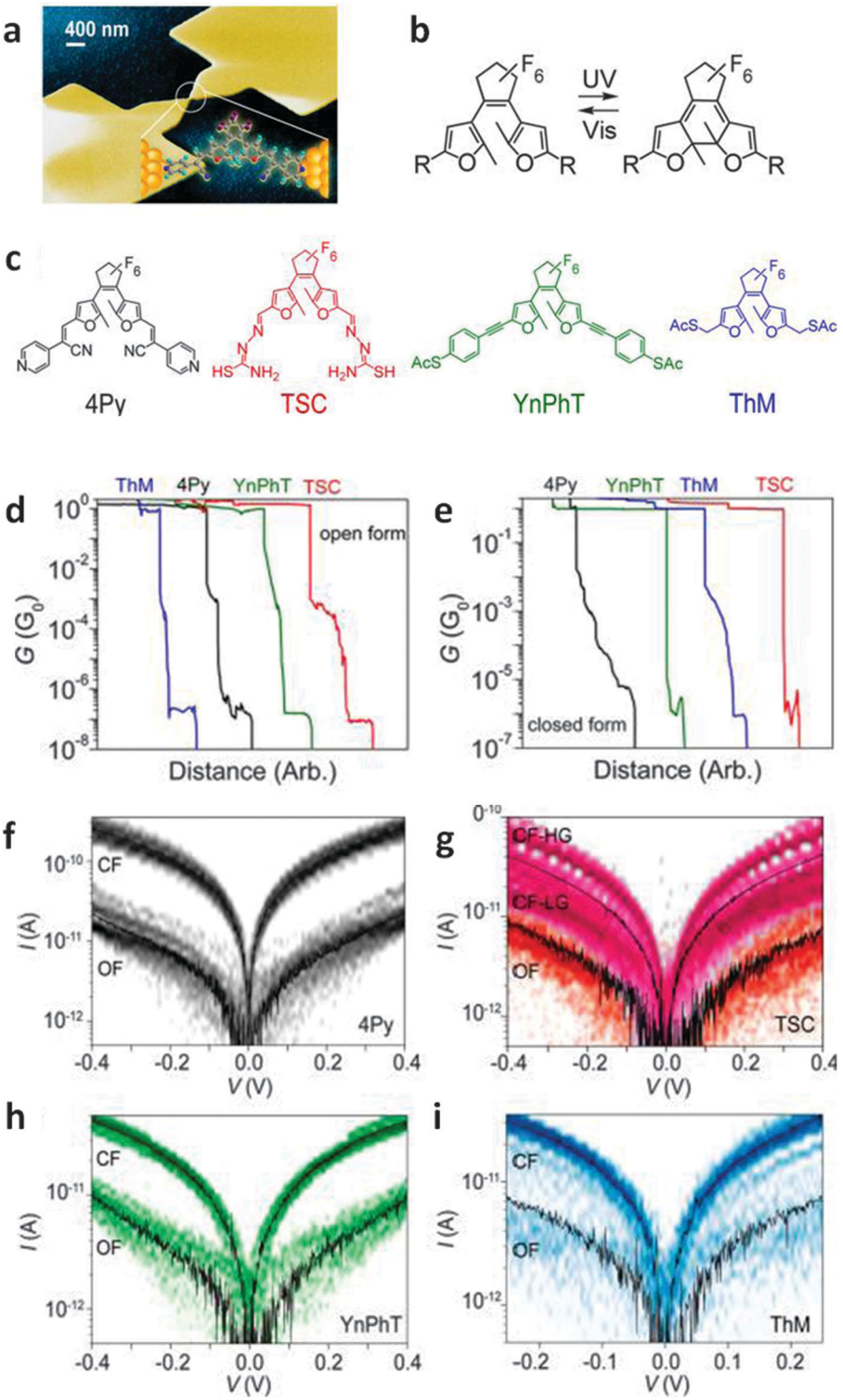

Fig. 16 (a) SEM image of the MCBJ device and an illustration of a Au–4Py–Au junction. (b) Sketches of open and closed forms of photochromic molecules (difurylethenes); R indicates the extended side chains and end groups. (c) Structures of the four different molecules, 4Py (black), TSC (red), YhPhT (green) and ThM (blue), measured in this study. (d) and (e) typical conductance-distance traces for open and closed forms of all four molecules as indicated in the panels. (f) Density plots of about 20 *I*–*V* curves of the open form (OF) and the closed form (CF) displayed for 4Py, (g) TSC, (h) YnPhT and (i) ThM. The density plots are obtained by 100 by 100 bins for *I* and *V*, and the color indicates counts in log-scale (minimum (white) is below 3 counts and maximum (dark color) is 60 counts). The solid curves are the averaged I–V_s for each isomer. In panel B, CF-HG and CF-LG indicate the high conductance and the low conductance states of closed TSC respectively, which is attributed to the coupling of TSC to gold *via* different end groups. Reprinted from ref. 201, with permission from American Chemical Society, copyright 2012.

 This journal is © The Royal Society of Chemistry 2015

Open Access Article. Published on 11 March 2015. Downloaded on 6/24/2024 3:25:25 PM.
This article is licensed under a Creative Commons Attribution 3.0 Unported Licence.

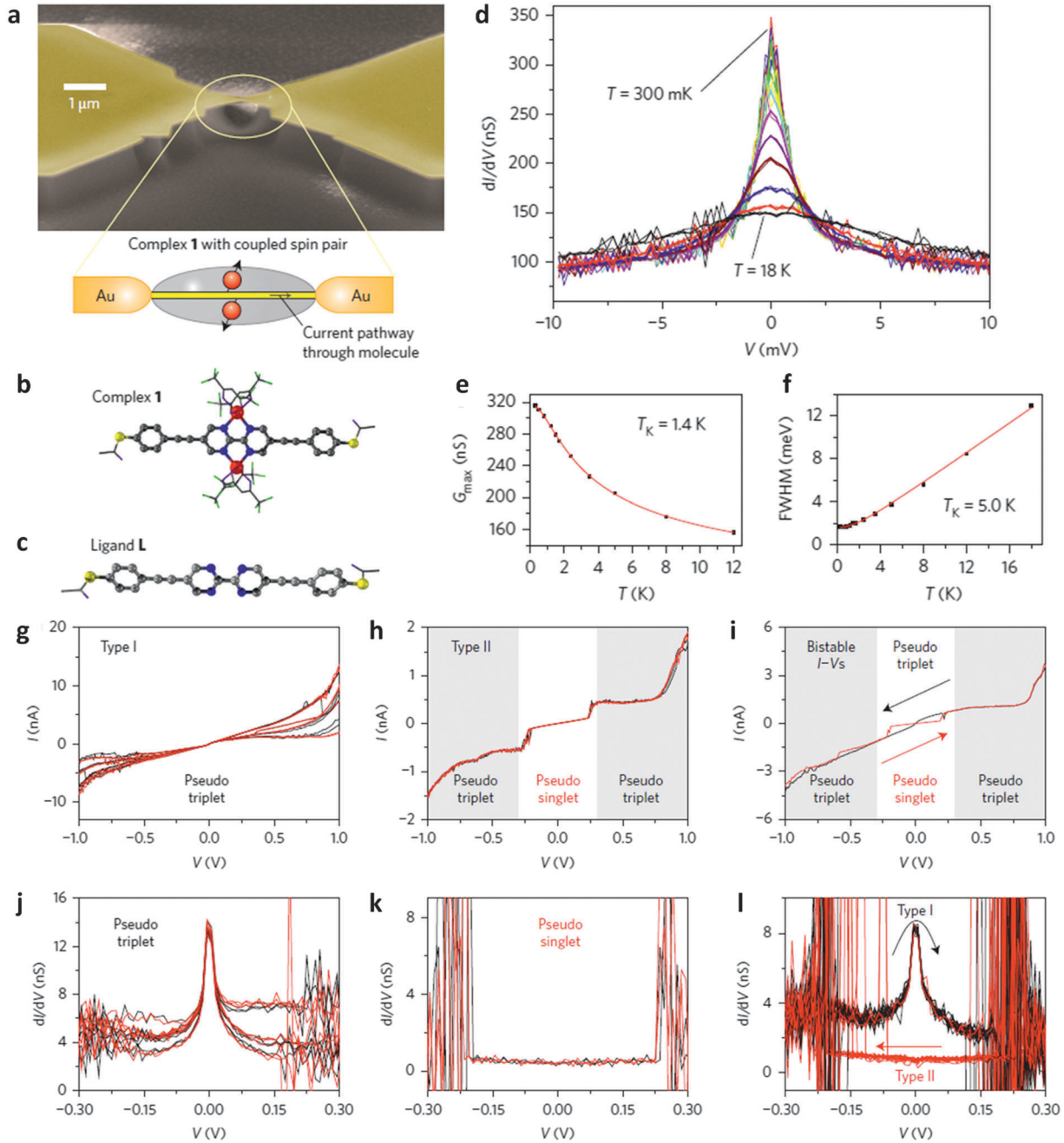

Fig. 17 (a) Scheme of the single molecule junction experiment. A molecule with a pair of spin center is contacted in a single molecule (SEM micrograph of a break junction set-up). The magnetic ion pair is attached orthogonally to the current pathway. (b) Molecular structure of complex 1 from single-crystal X-ray diffraction. The Co^{2+} ions are marked in red, carbon in grey, nitrogen in blue, oxygen in violet and sulphur in yellow, hydrogen atoms are omitted for clarity. (c) Molecular structure of bare bipyrimidine-wire L (for control experiments) from single-crystal X-ray diffraction. (d) Temperature dependence of the Kondo-like feature. (e) T_K = 1.4 K from a fit of the Kondo model (continuous line) to the data (black points) of the conductance maximum at zero bias. (f) FWHM measured *versus* temperature (black data points), fit by a Kondo model (continuous line), giving T_K = 5.0 K. (g) Type I *I*–*V* characteristics recorded at low temperatures and (j) the corresponding differential conductance obtained by numerical differentiation, many curves displays a Kondo-like zero bias anomaly. (h) Type II *I*–*V* characteristics with a discontinuity at ~2.0 V and (k) its numerical differentiation. (i) and (l) bistable *I*–*V* characteristics and the differential conductance due to hysteresis of the coupled spin pair. Down-sweeps are similar to (g) and up-sweeps to (h). Reprinted from ref. 195, with permission from Nature Publishing Group, copyright 2013.

the Au–ODT–Au junction. Fig. 18a shows the *I*–*V* characteristics for this single molecule transistor at different gate voltages V_G. It is found that the tunneling current increases as V_G becomes increasingly negative. The Fowler–Nordheim plot, which is an analysis of $\ln(I/V^2)$ *versus* $1/V$, is shown in Fig. 18b. Two distant transport regimes are separated by the transition voltage, as indicated by the arrows. The low-bias region with $V < V_{trans}$ is the direct tunneling region; while the high-bias region is the

Open Access Article. Published on 11 March 2015. Downloaded on 6/24/2024 3:25:25 PM.
This article is licensed under a Creative Commons Attribution 3.0 Unported Licence.

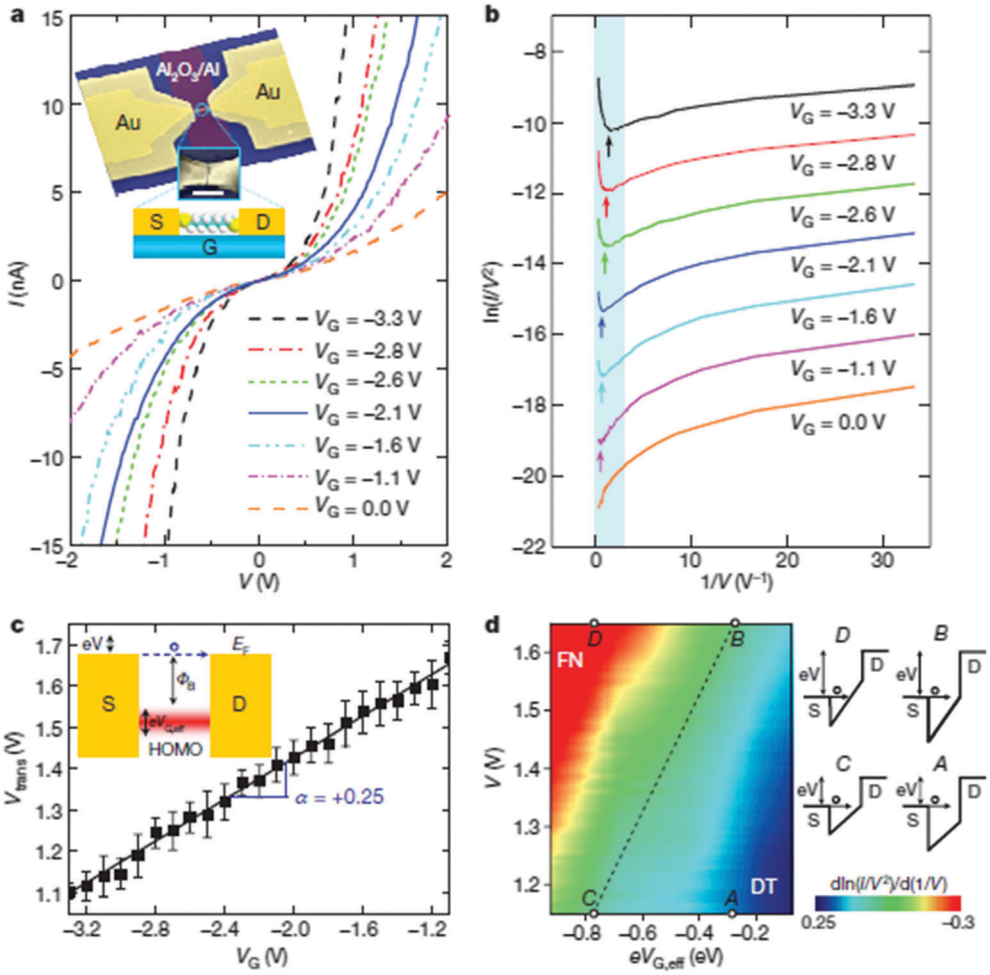

Fig. 18 Gate controlled charge transport characteristics of a Au–ODT–Au junction. (a) Representative I–V curves measured at 4.2 K for different values of V_G. Inset, the device structure and schematic. S, source; D, drain; G, gate. Scale bar, 100 nm. (b) Fowler–Nordheim plots corresponding to the I–V curves in (a), exhibiting the transition from direct to Fowler–Nordheim tunneling with a clear gate dependence. The plots are offset vertically for clarity purpose. The arrows indicate the boundaries between transport regimes. (c) Linear scaling of V_{trans} in terms of V_G. Inset, the schematic of the energy band for HOMO-mediated hole tunneling, where $eV_{G,eff}$ describes the actual amount of molecular orbital shift produced by gating. (d) Two-dimensional color map of $d\ln(I/V^2)/d(1/V)$ (from Fowler–Nordheim plots). Energy-band diagrams corresponding to four different regions (points A to D) are also shown. FN, Fowler–Nordheim tunneling; DT, direct tunneling. Reprinted from ref. 209, with permission from Nature Publishing Group, copyright 2009.

Fowler–Nordheim tunneling or field emission region. A controllable gate-voltage dependence of V_{trans} is observed in Fig. 18b and the plot of the V_{trans} against V_G reveals that V_{trans} scales linearly and reversibly as a function of V_G (Fig. 18c). The slope α is 0.25 here, which indicates that the molecular orbital energy changes by 0.25 eV when 1 V is applied to the gate electrode. Fig. 18d shows the two-dimensional color map of $d\ln(I/V^2)/d(1/V)$ as a function of V and $eV_{G,eff}$ ($V_{G,eff} = \alpha V_G$). The dashed line defines the boundary between the direct tunneling (DT) and Fowler–Nordheim tunneling (FN) regimes. Points A, B, C and D correspond to four different energy-band diagrams. At point A ($V < V_{trans}$), direct tunneling occurs across the trapezoidal barrier. Increasing the bias from V to V_{trans} (point B) results in a transition from the trapezoidal to the triangular barrier. This is the onset of FN tunneling. Point C also has a triangular barrier; however, as the V_{trans} is smaller at point C compared to that of point B, a smaller applied bias V is required to reach the on-set of FN tunneling. The tunneling at point D is dominated by FN tunneling as the applied bias V is larger than V_{trans}. The HOMO level relative to E_F in Au–ODT–Au junction is estimated to be 1.93 V by extrapolating the intercept from Fig. 18c at zero-gate voltage. These results indicate that the molecular orbital levels relative to E_F can be modulated by changing the gate voltage. The demonstration of this single molecule transistor could help pave the way towards the realization of molecular electronics.

5.4 Diodes

A diode, also called a rectifier, is a two-terminal device in which the current flow is allowed in the forward bias and blocked in the reverse bias. A single molecule rectifier is thus a voltage controlled single molecule switch. The first molecular diode was proposed by Aviram–Ratner, where a single molecule comprising a donor and an acceptor unit separated by a sigma

Open Access Article. Published on 11 March 2015. Downloaded on 6/24/2024 3:25:25 PM.
This article is licensed under a Creative Commons Attribution 3.0 Unported Licence.

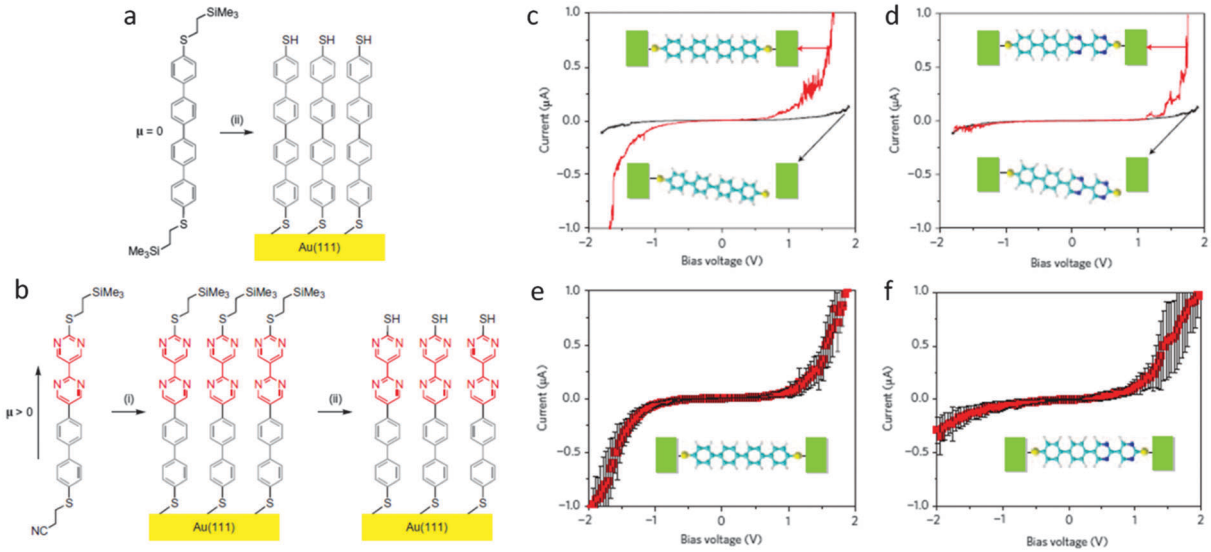

Fig. 19 (a) Symmetric tetraphenyl molecule and (b) non-symmetric dipyrimidinyl-diphenyl molecule. (c) The *I*–*V* curves recorded in the gap junction and single molecule junction for the symmetric tetraphenyl and (d) the non-symmetric dipyrimidinyl-diphenyl molecules. (e) Average curves for the single molecule junctions built from 30 and (f) 50 individual *I*–*V* curves. Reprinted from ref. 12, with permission from Nature Publishing Group, copyright 2009.

bonded tunneling bridge is expected to show rectifying properties.[1] During the past decades, the diode behavior in single molecules has been widely investigated.[12,189,194,198] To achieve a truly single molecule rectification effect, two terminals of the single molecule must be symmetrically bonded to the two electrodes with controlled orientation.

Using a selective deprotection strategy, Díez-Pérez *et al.* demonstrated that the non-symmetric diblock dipyrimidinyl-diphenyl molecule covalently bonded to a STM break junction exhibits pronounced rectification behavior.[12] Fig. 19a and b shows the molecular structures of the symmetric tetraphenyl and non-symmetric diblock dipyrimidinyldiphenyl molecules. In order to control the orientation of the non-symmetric molecule within the STM break junction, it is terminated with two different protecting groups, with the trimethylsilylethyl and cranoethyl attached to the dipyrimidinyl and diphenyl ends of the molecule, respectively. Initially, the cyanoethyl protecting group is removed from the molecule and a SAM with the diphenyl end bonded to the substrate electrode is formed. Then, the trimethylsilylethyl group is removed and the thiol group at the dipyrimidinyl end is exposed to the tip electrode. Fig. 19c and d show *I*–*V* curves recorded for the symmetric and non-symmetric molecules in both single molecule junction (upper panel) and gap junction (lower panel) configurations. In the single molecule junction, the end of the molecules are connected to the tip and substrate electrodes respectively; but in the gap junction, only one end of the molecule is connected to the substrate electrode. For the symmetric molecule, the *I*–*V* curves for both junction configurations are symmetric, as shown by the red curve and black curve in Fig. 19c. However, the *I*–*V* curves for the non-symmetric molecule bridged between the tip and the substrate display strong rectification (red curve in Fig. 19d). Fig. 19e and f are the average *I*–*V* curves for the symmetric and non-symmetric molecules in the single molecule junction configuration. This further confirms that the rectification effect in the non-symmetric molecule is not caused by the contact-induced non-symmetry but from the molecule itself. Measurements recorded with the non-symmetric molecules in the gap junction configuration (Fig. 19d, black curve) display symmetric *I*–*V* curves, which emphasizes the importance of the providing good contact at both ends of the molecule to observe the rectification effect.

6. Conclusions and outlook

In this article, we review recent progress of various molecular switches on surfaces and in single molecule junctions. Different external stimuli can be used to induce switching, and the molecular switches can be operated by different mechanisms according to their intrinsic properties. The STM is utilized as a powerful tool for real-space imaging, electronic structure characterization as well as single molecule manipulation. STM-based break junctions, MCBJs, and EBJs techniques are used to fabricate single molecules junctions. The great advantage of the molecular switches formed on the surface by self-assembly is that each molecule can be immobilized and isolated in a repetitive and spatially ordered manner. With the STM tip, an individual molecule can be addressed precisely and be controllably switched between different states. On the other hand, as one STM tip can only address one molecule each time, the operation for a task is very time-consuming. In this case, a parallel processing method that can address multiple molecules at the same time is required. Another main challenge of this kind of switches is their stability under ambient conditions. Inserting the tiol-terminated conjugated molecules into SAMs can create switches that are stable under ambient conditions, which is stabilized by the chemical bond between S–Au.

Open Access Article. Published on 11 March 2015. Downloaded on 6/24/2024 3:25:25 PM.
This article is licensed under a Creative Commons Attribution 3.0 Unported Licence.

However, as the molecules can only be inserted at the defect sites within the host films, these molecular switches are not well ordered on the surfaces. The advantage of switches in single molecule junctions is that they allow the realization of device functions such as single molecule diodes and single molecule field-effect transistors. However, the mass production of single molecule junctions is still a main challenge.

Though substantial progress has been made over the past decade, there are still major issues that need to be addressed. Most studies of molecular switches were performed either individually or in a self-assembled single-component monolayer. Wiring these molecular switches into more complex and rationally designed nano-architectures is needed for practical applications. To achieve this, single-molecular switches should be interconnected with other molecules. Hence, it is important to study the role of functional side groups on the chemical structure and the switching efficiency of the molecule. The precise control of the molecule-electrode contact is another major challenge. The supporting substrates play important roles in both defining the molecular adsorption geometry and molecule–substrate interaction, which could hinder or enable the switching process. Molecular adsorption on metallic surfaces results in strong electronic interactions with the reservoir of metal electrons, which can modify the intrinsic functionality of the molecules. For practical applications, we need to study these manipulations on inert substrates, such as graphite/graphene or ultra thin insulating films. Another problem involves the stability of these switches under ambient conditions. Most of the switching experiments are carried out at low temperature and in ultra-high-vacuum environments. The rational design of molecular switches with desired functionality, the formation of atomic/molecular interconnects, and the use of appropriate substrates are the next challenges for researchers in the field. A fundamental understanding of the underlying mechanism that governs the molecular switching process will require insights from the first principle calculations. The advancement of other SPM technologies, such as AFM and Kelvin probe force microscopy (KPFM), which can provide bond formation and charge distribution information in addition to atomic structure,[20,213,214] allow more accurate comparisons between theory and experiment. Molecular spectroscopy with submolecular spatial resolution has been realized by electroluminescence in STM (EL-STM) and Raman spectroscopy in STM (STM-RS). These vibronic shape resonances carry Fano line profiles which retain phase information, and hence the spectra can be transformed to the time domain. In this case, joint space-time resolution at the angstrom-femtosecond resolution can be achieved within a single molecule switch.[215] Future progress in these research areas will pave the way for the future development of single molecule technology.

Acknowledgements

The authors acknowledge the financial support from Singapore MOE grant R143-000-559-112, Singapore National Research Foundation CREATE-SPURc program R-143-001-205-592, Singapore NRF-CRP grant of "Doped Contacts and Heterostructures for Solution-Processable Plastic Electronics" under R143-001-608-281, National Key Basic Research Program of China (2015CB856505), Jiangsu Province Government Research Platform Grant and NUSRI Seed Fund.

References

1 A. Aviram and M. A. Ratner, *Chem. Phys. Lett.*, 1974, **29**, 277–283.
2 K. Szaciłowski, *Chem. Rev.*, 2008, **108**, 3481–3548.
3 J. Andréasson and U. Pischel, *Chem. Soc. Rev.*, 2010, **39**, 174–188.
4 M. Irie, T. Fukaminato, K. Matsuda and S. Kobatake, *Chem. Rev.*, 2014, **114**, 12174–12277.
5 M. A. Reed, C. Zhou, C. J. Muller, T. P. Burgin and J. M. Tour, *Science*, 1997, **278**, 252–254.
6 M. Di Ventra, S. T. Pantelides and N. D. Lang, *Phys. Rev. Lett.*, 2000, **84**, 979–982.
7 R. H. M. Smit, Y. Noat, C. Untiedt, N. D. Lang, M. C. van Hemert and J. M. van Ruitenbeek, *Nature*, 2002, **419**, 906–909.
8 J. Reichert, R. Ochs, D. Beckmann, H. B. Weber, M. Mayor and H. v. Löhneysen, *Phys. Rev. Lett.*, 2002, **88**, 176804.
9 B. Xu and N. J. Tao, *Science*, 2003, **301**, 1221–1223.
10 L. Venkataraman, J. E. Klare, C. Nuckolls, M. S. Hybertsen and M. L. Steigerwald, *Nature*, 2006, **442**, 904–907.
11 S. Y. Quek, M. Kamenetska, M. L. Steigerwald, H. J. Choi, S. G. Louie, M. S. Hybertsen, J. B. Neaton and L. Venkataraman, *Nat. Nanotechnol.*, 2009, **4**, 230–234.
12 I. Díez-Pérez, J. Hihath, Y. Lee, L. Yu, L. Adamska, M. A. Kozhushner, I. I. Oleynik and N. Tao, *Nat. Chem.*, 2009, **1**, 635–641.
13 H. Vazquez, R. Skouta, S. Schneebeli, M. Kamenetska, R. Breslow, L. Venkataraman and M. S. Hybertsen, *Nat. Nanotechnol.*, 2012, **7**, 663–667.
14 B. Xu, X. Xiao and N. J. Tao, *J. Am. Chem. Soc.*, 2003, **125**, 16164–16165.
15 D. R. Ward, N. J. Halas, J. W. Ciszek, J. M. Tour, Y. Wu, P. Nordlander and D. Natelson, *Nano Lett.*, 2008, **8**, 919–924.
16 X. H. Qiu, G. V. Nazin and W. Ho, *Science*, 2003, **299**, 542–546.
17 G. Binnig and H. Rohrer, *IBM J. Res. Dev.*, 2000, **44**, 279–293.
18 F. J. Giessibl, *Rev. Mod. Phys.*, 2003, **75**, 949–983.
19 A. Zhao, Q. Li, L. Chen, H. Xiang, W. Wang, S. Pan, B. Wang, X. Xiao, J. Yang, J. G. Hou and Q. Zhu, *Science*, 2005, **309**, 1542–1544.
20 J. Zhang, P. Chen, B. Yuan, W. Ji, Z. Cheng and X. Qiu, *Science*, 2013, **342**, 611–614.
21 M. Kiguchi, S. Nakashima, T. Tada, S. Watanabe, S. Tsuda, Y. Tsuji and J. Terao, *Small*, 2012, **8**, 726–730.
22 M. L. Perrin, C. J. O. Verzijl, C. A. Martin, A. J. Shaikh, R. Eelkema, J. H. van Esch, J. M. van Ruitenbeek,

Open Access Article. Published on 11 March 2015. Downloaded on 6/24/2024 3:25:25 PM.
This article is licensed under a Creative Commons Attribution 3.0 Unported Licence.

J. M. Thijssen, H. S. J. van der Zant and D. Dulić, *Nat. Nanotechnol.*, 2013, **8**, 282–287.
23 W. Liang, M. P. Shores, M. Bockrath, J. R. Long and H. Park, *Nature*, 2002, **417**, 725–729.
24 N. J. Tao, *Nat. Nanotechnol.*, 2006, **1**, 173–181.
25 Y. Selzer and D. L. Allara, *Annu. Rev. Phys. Chem.*, 2006, **57**, 593–623.
26 C. Joachim and M. A. Ratner, *Proc. Natl. Acad. Sci. U. S. A.*, 2005, **102**, 8801–8808.
27 S. V. Aradhya and L. Venkataraman, *Nat. Nanotechnol.*, 2013, **8**, 399–410.
28 *Nat. Nanotechnol.*, 2013, **8**, 377.
29 M. Ratner, *Nat. Nanotechnol.*, 2013, **8**, 378–381.
30 E. Lörtscher, *Nat. Nanotechnol.*, 2013, **8**, 381–384.
31 S. J. van der Molen, R. Naaman, E. Scheer, J. B. Neaton, A. Nitzan, D. Natelson, N. T. Tao, H. van der Zant, M. Mayor, M. Ruben, M. Reed and M. Calame, *Nat. Nanotechnol.*, 2013, **8**, 385–389.
32 H. J. Gao and L. Gao, *Prog. Surf. Sci.*, 2010, **85**, 28–91.
33 L. Gao, Q. Liu, Y. Y. Zhang, N. Jiang, H. G. Zhang, Z. H. Cheng, W. F. Qiu, S. X. Du, Y. Q. Liu, W. A. Hofer and H. J. Gao, *Phys. Rev. Lett.*, 2008, **101**, 197209.
34 M. Galperin and A. Nitzan, *Phys. Chem. Chem. Phys.*, 2012, **14**, 9421–9438.
35 Z. Liu, S. Y. Ding, Z. B. Chen, X. Wang, J. H. Tian, J. R. Anema, X. S. Zhou, D. Y. Wu, B. W. Mao, X. Xu, B. Ren and Z. Q. Tian, *Nat. Commun.*, 2011, **2**, 305.
36 G. Hoffmann, L. Libioulle and R. Berndt, *Phys. Rev. B: Condens. Matter Mater. Phys.*, 2002, **65**, 212107.
37 H. L. Tierney, C. J. Murphy, A. D. Jewell, A. E. Baber, E. V. Iski, H. Y. Khodaverdian, A. F. McGuire, N. Klebanov and E. C. H. Sykes, *Nat. Nanotechnol.*, 2011, **6**, 625–629.
38 T. Kudernac, N. Ruangsupapichat, M. Parschau, B. Maciá, N. Katsonis, S. R. Harutyunyan, K.-H. Ernst and B. L. Feringa, *Nature*, 2011, **479**, 208–211.
39 L. Grill, K. H. Rieder, F. Moresco, G. Rapenne, S. Stojkovic, X. Bouju and C. Joachim, *Nat. Nanotechnol.*, 2007, **2**, 95–98.
40 S. Sanvito, *Chem. Soc. Rev.*, 2011, **40**, 3336–3355.
41 L. Bogani and W. Wernsdorfer, *Nat. Mater.*, 2008, **7**, 179–186.
42 H. B. Heersche, Z. de Groot, J. A. Folk, H. S. J. van der Zant, C. Romeike, M. R. Wegewijs, L. Zobbi, D. Barreca, E. Tondello and A. Cornia, *Phys. Rev. Lett.*, 2006, **96**, 206801.
43 E. A. Osorio, K. Moth-Poulsen, H. S. J. van der Zant, J. Paaske, P. Hedegård, K. Flensberg, J. Bendix and T. Bjørnholm, *Nano Lett.*, 2010, **10**, 105–110.
44 S. Schmaus, A. Bagrets, Y. Nahas, T. K. Yamada, A. Bork, M. Bowen, E. Beaurepaire, F. Evers and W. Wulfhekel, *Nat. Nanotechnol.*, 2011, **6**, 185–189.
45 C. Iacovita, M. V. Rastei, B. W. Heinrich, T. Brumme, J. Kortus, L. Limot and J. P. Bucher, *Phys. Rev. Lett.*, 2008, **101**, 116602.
46 R. Vincent, S. Klyatskaya, M. Ruben, W. Wernsdorfer and F. Balestro, *Nature*, 2012, **488**, 357–360.
47 A. R. Rocha, V. M. García-suárez, S. W. Bailey, C. J. Lambert, J. Ferrer and S. Sanvito, *Nat. Mater.*, 2005, **4**, 335–339.
48 G. Guillaud, J. Simon and J. P. Germain, *Coord. Chem. Rev.*, 1998, **178–180**(part 2), 1433–1484.
49 N. A. Rakow and K. S. Suslick, *Nature*, 2000, **406**, 710–713.
50 F. I. Bohrer, A. Sharoni, C. Colesniuc, J. Park, I. K. Schuller, A. C. Kummel and W. C. Trogler, *J. Am. Chem. Soc.*, 2007, **129**, 5640–5646.
51 T. G. Gopakumar, H. Tang, J. Morillo and R. Berndt, *J. Am. Chem. Soc.*, 2012, **134**, 11844–11847.
52 X. H. Qiu, G. V. Nazin and W. Ho, *Phys. Rev. Lett.*, 2004, **93**, 196806.
53 P. Liljeroth, J. Repp and G. Meyer, *Science*, 2007, **317**, 1203–1206.
54 J. Henzl, M. Mehlhorn, H. Gawronski, K.-H. Rieder and K. Morgenstern, *Angew. Chem., Int. Ed.*, 2006, **45**, 603–606.
55 B.-Y. Choi, S.-J. Kahng, S. Kim, H. Kim, H. W. Kim, Y. J. Song, J. Ihm and Y. Kuk, *Phys. Rev. Lett.*, 2006, **96**, 156106.
56 Y. Wang, J. Kröger, R. Berndt and W. A. Hofer, *J. Am. Chem. Soc.*, 2009, **131**, 3639–3643.
57 N. Pavliček, B. Fleury, M. Neu, J. Niedenführ, C. Herranz-Lancho, M. Ruben and J. Repp, *Phys. Rev. Lett.*, 2012, **108**, 086101.
58 T. Leoni, O. Guillermet, H. Walch, V. Langlais, A. Scheuermann, J. Bonvoisin and S. Gauthier, *Phys. Rev. Lett.*, 2011, **106**, 216103.
59 S. W. Wu, N. Ogawa and W. Ho, *Science*, 2006, **312**, 1362–1365.
60 Y.-S. Fu, T. Zhang, S.-H. Ji, X. Chen, X.-C. Ma, J.-F. Jia and Q.-K. Xue, *Phys. Rev. Lett.*, 2009, **103**, 257202.
61 I. Swart, T. Sonnleitner and J. Repp, *Nano Lett.*, 2011, **11**, 1580–1584.
62 F. Mohn, J. Repp, L. Gross, G. Meyer, M. S. Dyer and M. Persson, *Phys. Rev. Lett.*, 2010, **105**, 266102.
63 J. Repp, G. Meyer, F. E. Olsson and M. Persson, *Science*, 2004, **305**, 493–495.
64 Z. J. Donhauser, B. A. Mantooth, K. F. Kelly, L. A. Bumm, J. D. Monnell, J. J. Stapleton, D. W. Price, A. M. Rawlett, D. L. Allara, J. M. Tour and P. S. Weiss, *Science*, 2001, **292**, 2303–2307.
65 H. Yanagi, K. Ikuta, H. Mukai and T. Shibutani, *Nano Lett.*, 2002, **2**, 951–955.
66 M. Alemani, M. V. Peters, S. Hecht, K.-H. Rieder, F. Moresco and L. Grill, *J. Am. Chem. Soc.*, 2006, **128**, 14446–14447.
67 C. P. Collier, G. Mattersteig, E. W. Wong, Y. Luo, K. Beverly, J. Sampaio, F. M. Raymo, J. F. Stoddart and J. R. Heath, *Science*, 2000, **289**, 1172–1175.
68 M. Lastapis, M. Martin, D. Riedel, L. Hellner, G. Comtet and G. Dujardin, *Science*, 2005, **308**, 1000–1003.
69 G. Pace, V. Ferri, C. Grave, M. Elbing, C. von Hänisch, M. Zharnikov, M. Mayor, M. A. Rampi and P. Samorì, *Proc. Natl. Acad. Sci. U. S. A.*, 2007, **104**, 9937–9942.
70 F. Moresco, G. Meyer, K.-H. Rieder, H. Tang, A. Gourdon and C. Joachim, *Phys. Rev. Lett.*, 2001, **86**, 672–675.
71 V. Iancu, A. Deshpande and S.-W. Hla, *Nano Lett.*, 2006, **6**, 820–823.

Open Access Article. Published on 11 March 2015. Downloaded on 6/24/2024 3:25:25 PM.
This article is licensed under a Creative Commons Attribution 3.0 Unported Licence.

72 M. J. Comstock, N. Levy, A. Kirakosian, J. Cho, F. Lauterwasser, J. H. Harvey, D. A. Strubbe, J. M. J. Fréchet, D. Trauner, S. G. Louie and M. F. Crommie, *Phys. Rev. Lett.*, 2007, **99**, 038301.
73 M. Parschau, D. Passerone, K.-H. Rieder, H. J. Hug and K.-H. Ernst, *Angew. Chem., Int. Ed.*, 2009, **48**, 4065–4068.
74 T. Miyamachi, M. Gruber, V. Davesne, M. Bowen, S. Boukari, L. Joly, F. Scheurer, G. Rogez, T. K. Yamada, P. Ohresser, E. Beaurepaire and W. Wulfhekel, *Nat. Commun.*, 2012, **3**, 938.
75 T. G. Gopakumar, F. Matino, H. Naggert, A. Bannwarth, F. Tuczek and R. Berndt, *Angew. Chem., Int. Ed.*, 2012, **51**, 6262–6266.
76 C. Uhlmann, I. Swart and J. Repp, *Nano Lett.*, 2013, **13**, 777–780.
77 V. Iancu and S.-W. Hla, *Proc. Natl. Acad. Sci. U. S. A.*, 2006, **103**, 13718–13721.
78 W. Auwärter, K. Seufert, F. Bischoff, D. Ecija, S. Vijayaraghavan, S. Joshi, F. Klappenberger, N. Samudrala and J. V. Barth, *Nat. Nanotechnol.*, 2012, **7**, 41–46.
79 M. J. Comstock, D. A. Strubbe, L. Berbil-Bautista, N. Levy, J. Cho, D. Poulsen, J. M. J. Fréchet, S. G. Louie and M. F. Crommie, *Phys. Rev. Lett.*, 2010, **104**, 178301.
80 S. Weigelt, C. Busse, L. Petersen, E. Rauls, B. Hammer, K. V. Gothelf, F. Besenbacher and T. R. Linderoth, *Nat. Mater.*, 2006, **5**, 112–117.
81 K. Morgenstern, *Acc. Chem. Res.*, 2009, **42**, 213–223.
82 S. W. Wu, N. Ogawa, G. V. Nazin and W. Ho, *J. Phys. Chem. C*, 2008, **112**, 5241–5244.
83 Y.-S. Fu, J. Schwöbel, S.-W. Hla, A. Dilullo, G. Hoffmann, S. Klyatskaya, M. Ruben and R. Wiesendanger, *Nano Lett.*, 2012, **12**, 3931–3935.
84 S. J. van der Molen and P. Liljeroth, *J. Phys.: Condens. Matter*, 2010, **22**, 133001.
85 L. Grill, *J. Phys.: Condens. Matter*, 2008, **20**, 053001.
86 S.-W. Hla and K.-H. Rieder, *Annu. Rev. Phys. Chem.*, 2003, **54**, 307–330.
87 T. Niu and A. Li, *J. Phys. Chem. Lett.*, 2013, **4**, 4095–4102.
88 T. Komeda, *Prog. Surf. Sci.*, 2005, **78**, 41–85.
89 K. Morgenstern, N. Lorente and K.-H. Rieder, *Phys. Status Solidi B*, 2013, **250**, 1671–1751.
90 K. Yang, L. Liu, L. Zhang, W. Xiao, X. Fei, H. Chen, S. Du, K.-H. Ernst and H.-J. Gao, *ACS Nano*, 2014, **8**, 2246–2251.
91 N. Katsonis, M. Lubomska, M. M. Pollard, B. L. Feringa and P. Rudolf, *Prog. Surf. Sci.*, 2007, **82**, 407–434.
92 K. Morgenstern, *Prog. Surf. Sci.*, 2011, **86**, 115–161.
93 C. Dri, M. V. Peters, J. Schwarz, S. Hecht and L. Grill, *Nat. Nanotechnol.*, 2008, **3**, 649–653.
94 G. London, G. T. Carroll, T. Fernández Landaluce, M. M. Pollard, P. Rudolf and B. L. Feringa, *Chem. Commun.*, 2009, 1712–1714.
95 W. R. Browne and B. L. Feringa, *Annu. Rev. Phys. Chem.*, 2009, **60**, 407–428.
96 J. J. Davis, G. A. Orlowski, H. Rahman and P. D. Beer, *Chem. Commun.*, 2010, **46**, 54–63.
97 J. L. Zhang, J. L. Xu, T. C. Niu, Y. H. Lu, L. Liu and W. Chen, *J. Phys. Chem. C*, 2014, **118**, 1712–1718.
98 Y. L. Huang, Y. Lu, T. C. Niu, H. Huang, S. Kera, N. Ueno, A. T. S. Wee and W. Chen, *Small*, 2012, **8**, 1423–1428.
99 J. L. Zhang, T. C. Niu, A. T. S. Wee and W. Chen, *Phys. Chem. Chem. Phys.*, 2013, **15**, 12414–12427.
100 L. Liu, K. Yang, Y. Jiang, B. Song, W. Xiao, L. Li, H. Zhou, Y. Wang, S. Du, M. Ouyang, W. A. Hofer, A. H. Castro Neto and H.-J. Gao, *Sci. Rep.*, 2013, **3**, 1210.
101 A. Stróżecka, M. Soriano, J. I. Pascual and J. J. Palacios, *Phys. Rev. Lett.*, 2012, **109**, 147202.
102 M. del Valle, R. Gutierrez, C. Tejedor and G. Cuniberti, *Nat. Nanotechnol.*, 2007, **2**, 176–179.
103 M. Wolf and P. Tegeder, *Surf. Sci.*, 2009, **603**, 1506–1517.
104 H. Rau and E. Lueddecke, *J. Am. Chem. Soc.*, 1982, **104**, 1616–1620.
105 I. K. Lednev, T.-Q. Ye, R. E. Hester and J. N. Moore, *J. Phys. Chem.*, 1996, **100**, 13338–13341.
106 A. Cembran, F. Bernardi, M. Garavelli, L. Gagliardi and G. Orlandi, *J. Am. Chem. Soc.*, 2004, **126**, 3234–3243.
107 I. K. Lednev, T. Q. Ye, P. Matousek, M. Towrie, P. Foggi, F. V. R. Neuwahl, S. Umapathy, R. E. Hester and J. N. Moore, *Chem. Phys. Lett.*, 1998, **290**, 68–74.
108 C. R. Crecca and A. E. Roitberg, *J. Phys. Chem. A*, 2006, **110**, 8188–8203.
109 S. Hagen, P. Kate, F. Leyssner, D. Nandi, M. Wolf and P. Tegeder, *J. Chem. Phys.*, 2008, **129**, 164102.
110 T. Ikeda and O. Tsutsumi, *Science*, 1995, **268**, 1873–1875.
111 Y. Yu, M. Nakano and T. Ikeda, *Nature*, 2003, **425**, 145.
112 T. Hugel, N. B. Holland, A. Cattani, L. Moroder, M. Seitz and H. E. Gaub, *Science*, 2002, **296**, 1103–1106.
113 R. D. Ramsier and J. T. Yates Jr, *Surf. Sci. Rep.*, 1991, **12**, 246–378.
114 H. Petek, *J. Chem. Phys.*, 2012, **137**, 091704.
115 J. W. Gadzuk and C. W. Clark, *J. Chem. Phys.*, 1989, **91**, 3174–3181.
116 J. A. Misewich, T. F. Heinz and D. M. Newns, *Phys. Rev. Lett.*, 1992, **68**, 3737–3740.
117 J. W. Gadzuk, *Phys. Rev. B: Condens. Matter Mater. Phys.*, 1991, **44**, 13466–13477.
118 L. Bartels, G. Meyer, K. H. Rieder, D. Velic, E. Knoesel, A. Hotzel, M. Wolf and G. Ertl, *Phys. Rev. Lett.*, 1998, **80**, 2004–2007.
119 B. C. Stipe, M. A. Rezaei, W. Ho, S. Gao, M. Persson and B. I. Lundqvist, *Phys. Rev. Lett.*, 1997, **78**, 4410–4413.
120 T. Komeda, Y. Kim, M. Kawai, B. N. J. Persson and H. Ueba, *Science*, 2002, **295**, 2055–2058.
121 B. C. Stipe, M. A. Rezaei and W. Ho, *Phys. Rev. Lett.*, 1998, **81**, 1263–1266.
122 T. Komeda, Y. Kim, Y. Fujita, Y. Sainoo and M. Kawai, *J. Chem. Phys.*, 2004, **120**, 5347–5352.
123 L. Chen, H. Li and A. T. S. Wee, *ACS Nano*, 2009, **3**, 3684–3690.
124 R. E. Palmer, *Prog. Surf. Sci.*, 1992, **41**, 51–108.
125 T. Huang, J. Zhao, M. Feng, A. A. Popov, S. Yang, L. Dunsch and H. Petek, *Nano Lett.*, 2011, **11**, 5327–5332.

Open Access Article. Published on 11 March 2015. Downloaded on 6/24/2024 3:25:25 PM.
This article is licensed under a Creative Commons Attribution 3.0 Unported Licence.

126 M. F. Perutz, *Nature*, 1970, **228**, 726–734.
127 K. J. Albert, N. S. Lewis, C. L. Schauer, G. A. Sotzing, S. E. Stitzel, T. P. Vaid and D. R. Walt, *Chem. Rev.*, 2000, **100**, 2595–2626.
128 J. D. Wright, *Prog. Surf. Sci.*, 1989, **31**, 1–60.
129 K. Flechtner, A. Kretschmann, H.-P. Steinrück and J. M. Gottfried, *J. Am. Chem. Soc.*, 2007, **129**, 12110–12111.
130 W. Hieringer, K. Flechtner, A. Kretschmann, K. Seufert, W. Auwärter, J. V. Barth, A. Görling, H.-P. Steinrück and J. M. Gottfried, *J. Am. Chem. Soc.*, 2011, **133**, 6206–6222.
131 J. Miguel, C. F. Hermanns, M. Bernien, A. Krüger and W. Kuch, *J. Phys. Chem. Lett.*, 2011, **2**, 1455–1459.
132 C. Isvoranu, B. Wang, E. Ataman, J. Knudsen, K. Schulte, J. N. Andersen, M.-L. Bocquet and J. Schnadt, *J. Phys. Chem. C*, 2011, **115**, 24718–24727.
133 C. Wäckerlin, D. Chylarecka, A. Kleibert, K. Müller, C. Iacovita, F. Nolting, T. A. Jung and N. Ballav, *Nat. Commun.*, 2010, **1**, 61.
134 I. Mochida, K. Suetsugu, H. Fujitsu and K. Takeshita, *J. Phys. Chem.*, 1983, **87**, 1524–1529.
135 Y.-S. Fu, S.-H. Ji, X. Chen, X.-C. Ma, R. Wu, C.-C. Wang, W.-H. Duan, X.-H. Qiu, B. Sun, P. Zhang, J.-F. Jia and Q.-K. Xue, *Phys. Rev. Lett.*, 2007, **99**, 256601.
136 L. Gao, W. Ji, Y. B. Hu, Z. H. Cheng, Z. T. Deng, Q. Liu, N. Jiang, X. Lin, W. Guo, S. X. Du, W. A. Hofer, X. C. Xie and H. J. Gao, *Phys. Rev. Lett.*, 2007, **99**, 106402.
137 K. J. Franke, G. Schulze and J. I. Pascual, *Science*, 2011, **332**, 940–944.
138 A. Mugarza, C. Krull, R. Robles, S. Stepanow, G. Ceballos and P. Gambardella, *Nat. Commun.*, 2011, **2**, 490.
139 S. Schintke and W.-D. Schneider, *J. Phys.: Condens. Matter*, 2004, **16**, R49.
140 H. J. Lee and W. Ho, *Science*, 1999, **286**, 1719–1722.
141 R. Zhang, Y. Zhang, Z. C. Dong, S. Jiang, C. Zhang, L. G. Chen, L. Zhang, Y. Liao, J. Aizpurua, Y. Luo, J. L. Yang and J. G. Hou, *Nature*, 2013, **498**, 82–86.
142 F. Besenbacher, J. V. Lauritsen, T. R. Linderoth, E. Lægsgaard, R. T. Vang and S. Wendt, *Surf. Sci.*, 2009, **603**, 1315–1327.
143 T. C. Niu, Y. L. Huang, J. T. Sun, S. Kera, N. Ueno, A. T. S. Wee and W. Chen, *Appl. Phys. Lett.*, 2011, **99**, 143114.
144 J. A. Theobald, N. S. Oxtoby, M. A. Phillips, N. R. Champness and P. H. Beton, *Nature*, 2003, **424**, 1029–1031.
145 Y. Wang, J. Kröger, R. Berndt and W. A. Hofer, *J. Am. Chem. Soc.*, 2009, **131**, 3639–3643.
146 T. Komeda, H. Isshiki, J. Liu, Y.-F. Zhang, N. Lorente, K. Katoh, B. K. Breedlove and M. Yamashita, *Nat. Commun.*, 2011, **2**, 217.
147 H. Fukagawa, S. Hosoumi, H. Yamane, S. Kera and N. Ueno, *Phys. Rev. B: Condens. Matter Mater. Phys.*, 2011, **83**, 085304.
148 A. Natan, L. Kronik, H. Haick and R. T. Tung, *Adv. Mater.*, 2007, **19**, 4103–4117.
149 G. Ashkenasy, D. Cahen, R. Cohen, A. Shanzer and A. Vilan, *Acc. Chem. Res.*, 2002, **35**, 121–128.
150 H. Y. Mao, R. Wang, Y. Wang, T. C. Niu, J. Q. Zhong, M. Y. Huang, D. C. Qi, K. P. Loh, A. T. S. Wee and W. Chen, *Appl. Phys. Lett.*, 2011, **99**, 093301.
151 Y. L. Huang, W. Chen, F. Bussolotti, T. C. Niu, A. T. S. Wee, N. Ueno and S. Kera, *Phys. Rev. B: Condens. Matter Mater. Phys.*, 2013, **87**, 085205.
152 J. L. Zhang, Z. Z. Wang, T. C. Niu, Z. Y. Li and W. Chen, *Appl. Phys. Lett.*, 2014, **104**, 113506.
153 Y. H. Jiang, W. D. Xiao, L. W. Liu, L. Z. Zhang, J. C. Lian, K. Yang, S. X. Du and H. J. Gao, *J. Phys. Chem. C*, 2011, **115**, 21750–21754.
154 J. R. Friedman, M. P. Sarachik, J. Tejada and R. Ziolo, *Phys. Rev. Lett.*, 1996, **76**, 3830–3833.
155 L. Lecren, W. Wernsdorfer, Y.-G. Li, O. Roubeau, H. Miyasaka and R. Clérac, *J. Am. Chem. Soc.*, 2005, **127**, 11311–11317.
156 J. Park, A. N. Pasupathy, J. I. Goldsmith, C. Chang, Y. Yaish, J. R. Petta, M. Rinkoski, J. P. Sethna, H. D. Abruña, P. L. McEuen and D. C. Ralph, *Nature*, 2002, **417**, 722–725.
157 G.-H. Kim and T.-S. Kim, *Phys. Rev. Lett.*, 2004, **92**, 137203.
158 T. Komeda, K. Katoh and M. Yamashita, *Prog. Surf. Sci.*, 2014, **89**, 127–160.
159 J. Kondo, *Phys. Rev.*, 1968, **169**, 437–440.
160 H. Jeong, A. M. Chang and M. R. Melloch, *Science*, 2001, **293**, 2221–2223.
161 V. Madhavan, W. Chen, T. Jamneala, M. F. Crommie and N. S. Wingreen, *Science*, 1998, **280**, 567–569.
162 F. E. Olsson, S. Paavilainen, M. Persson, J. Repp and G. Meyer, *Phys. Rev. Lett.*, 2007, **98**, 176803.
163 G. Decher, *Angew. Chem.*, 1992, **104**, 498–499.
164 C. E. D. Chidsey and D. N. Loiacono, *Langmuir*, 1990, **6**, 682–691.
165 W. S. V. Kwan, L. Atanasoska and L. L. Miller, *Langmuir*, 1991, **7**, 1419–1425.
166 R. K. Smith, P. A. Lewis and P. S. Weiss, *Prog. Surf. Sci.*, 2004, **75**, 1–68.
167 Z. J. Donhauser, B. A. Mantooth, T. P. Pearl, K. F. Kelly, S. U. Nanayakkara and P. S. Weiss, *Jpn. J. Appl. Phys.*, 2002, **41**, 4871.
168 P. A. Lewis, C. E. Inman, Y. Yao, J. M. Tour, J. E. Hutchison and P. S. Weiss, *J. Am. Chem. Soc.*, 2004, **126**, 12214–12215.
169 P. A. Lewis, C. E. Inman, F. Maya, J. M. Tour, J. E. Hutchison and P. S. Weiss, *J. Am. Chem. Soc.*, 2005, **127**, 17421–17426.
170 R. A. Wassel, R. R. Fuierer, N. Kim and C. B. Gorman, *Nano Lett.*, 2003, **3**, 1617–1620.
171 G. K. Ramachandran, T. J. Hopson, A. M. Rawlett, L. A. Nagahara, A. Primak and S. M. Lindsay, *Science*, 2003, **300**, 1413–1416.
172 H. Sakaguchi, H. Matsumura and H. Gong, *Nat. Mater.*, 2004, **3**, 551–557.
173 A. A. Dameron, J. W. Ciszek, J. M. Tour and P. S. Weiss, *J. Phys. Chem. B*, 2004, **108**, 16761–16767.
174 L. A. Bumm, J. J. Arnold, M. T. Cygan, T. D. Dunbar, T. P. Burgin, L. Jones, D. L. Allara, J. M. Tour and P. S. Weiss, *Science*, 1996, **271**, 1705–1707.

Open Access Article. Published on 11 March 2015. Downloaded on 6/24/2024 3:25:25 PM.
This article is licensed under a Creative Commons Attribution 3.0 Unported Licence.

175 M. P. Samanta, W. Tian, S. Datta, J. I. Henderson and C. P. Kubiak, *Phys. Rev. B: Condens. Matter Mater. Phys.*, 1996, **53**, R7626–R7629.
176 J. Chen, M. A. Reed, A. M. Rawlett and J. M. Tour, *Science*, 1999, **286**, 1550–1552.
177 J. Chen, W. Wang, M. A. Reed, A. M. Rawlett, D. W. Price and J. M. Tour, *Appl. Phys. Lett.*, 2000, **77**, 1224–1226.
178 J. M. Seminario, A. G. Zacarias and J. M. Tour, *J. Am. Chem. Soc.*, 2000, **122**, 3015–3020.
179 M. Di Ventra, S. G. Kim, S. T. Pantelides and N. D. Lang, *Phys. Rev. Lett.*, 2001, **86**, 288–291.
180 J. Cornil, Y. Karzazi and J. L. Brédas, *J. Am. Chem. Soc.*, 2002, **124**, 3516–3517.
181 N. D. Lang and Ph. Avouris, *Phys. Rev. B: Condens. Matter Mater. Phys.*, 2000, **62**, 7325–7329.
182 J. M. Seminario, A. G. Zacarias and J. M. Tour, *J. Am. Chem. Soc.*, 1998, **120**, 3970–3974.
183 H. Sellers, A. Ulman, Y. Shnidman and J. E. Eilers, *J. Am. Chem. Soc.*, 1993, **115**, 9389–9401.
184 Y.-T. Tao, C.-C. Wu, J.-Y. Eu, W.-L. Lin, K.-C. Wu and C.-h. Chen, *Langmuir*, 1997, **13**, 4018–4023.
185 B. K. Pathem, S. A. Claridge, Y. B. Zheng and P. S. Weiss, *Annu. Rev. Phys. Chem.*, 2013, **64**, 605–630.
186 A. M. Moore, A. A. Dameron, B. A. Mantooth, R. K. Smith, D. J. Fuchs, J. W. Ciszek, F. Maya, Y. Yao, J. M. Tour and P. S. Weiss, *J. Am. Chem. Soc.*, 2006, **128**, 1959–1967.
187 L. Sun, Y. A. Diaz-Fernandez, T. A. Gschneidtner, F. Westerlund, S. Lara-Avila and K. Moth-Poulsen, *Chem. Soc. Rev.*, 2014, **43**, 7378–7411.
188 M. Kiguchi, T. Ohto, S. Fujii, K. Sugiyasu, S. Nakajima, M. Takeuchi and H. Nakamura, *J. Am. Chem. Soc.*, 2014, **136**, 7327–7332.
189 A. Batra, P. Darancet, Q. Chen, J. S. Meisner, J. R. Widawsky, J. B. Neaton, C. Nuckolls and L. Venkataraman, *Nano Lett.*, 2013, **13**, 6233–6237.
190 X. Xiao, B. Xu and N. J. Tao, *Nano Lett.*, 2004, **4**, 267–271.
191 C. Bruot, J. Hihath and N. Tao, *Nat. Nanotechnol.*, 2012, **7**, 35–40.
192 C. Li, I. Pobelov, T. Wandlowski, A. Bagrets, A. Arnold and F. Evers, *J. Am. Chem. Soc.*, 2008, **130**, 318–326.
193 D. Xiang, H. Jeong, D. Kim, T. Lee, Y. Cheng, Q. Wang and D. Mayer, *Nano Lett.*, 2013, **13**, 2809–2813.
194 M. Elbing, R. Ochs, M. Koentopp, M. Fischer, C. von Hänisch, F. Weigend, F. Evers, H. B. Weber and M. Mayor, *Proc. Natl. Acad. Sci. U. S. A.*, 2005, **102**, 8815–8820.
195 S. Wagner, F. Kisslinger, S. Ballmann, F. Schramm, R. Chandrasekar, T. Bodenstein, O. Fuhr, D. Secker, K. Fink, M. Ruben and H. B. Weber, *Nat. Nanotechnol.*, 2013, **8**, 575–579.
196 E. Lörtscher, J. W. Ciszek, J. Tour and H. Riel, *Small*, 2006, **2**, 973–977.
197 M. Taniguchi, M. Tsutsui, K. Yokota and T. Kawai, *Chem. Sci.*, 2010, **1**, 247–253.
198 E. Lörtscher, B. Gotsmann, Y. Lee, L. Yu, C. Rettner and H. Riel, *ACS Nano*, 2012, **6**, 4931–4939.
199 D. Xiang, H. Jeong, T. Lee and D. Mayer, *Adv. Mater.*, 2013, **25**, 4845–4867.
200 C. A. Martin, R. H. M. Smit, H. S. J. van der Zant and J. M. van Ruitenbeek, *Nano Lett.*, 2009, **9**, 2940–2945.
201 Y. Kim, T. J. Hellmuth, D. Sysoiev, F. Pauly, T. Pietsch, J. Wolf, A. Erbe, T. Huhn, U. Groth, U. E. Steiner and E. Scheer, *Nano Lett.*, 2012, **12**, 3736–3742.
202 H. Park, A. K. L. Lim, A. P. Alivisatos, J. Park and P. L. McEuen, *Appl. Phys. Lett.*, 1999, **75**, 301–303.
203 H. Park, J. Park, A. K. L. Lim, E. H. Anderson, A. P. Alivisatos and P. L. McEuen, *Nature*, 2000, **407**, 57–60.
204 L. H. Yu and D. Natelson, *Nano Lett.*, 2004, **4**, 79–83.
205 H. Yu, Y. Luo, K. Beverly, J. F. Stoddart, H.-R. Tseng and J. R. Heath, *Angew. Chem., Int. Ed.*, 2003, **42**, 5706–5711.
206 D. E. Johnston, D. R. Strachan and A. T. C. Johnson, *Nano Lett.*, 2007, **7**, 2774–2777.
207 D. Stöffler, S. Fostner, P. Grütter and R. Hoffmann-Vogel, *Phys. Rev. B: Condens. Matter Mater. Phys.*, 2012, **85**, 033404.
208 D. R. Ward, F. Hüser, F. Pauly, J. C. Cuevas and D. Natelson, *Nat. Nanotechnol.*, 2010, **5**, 732–736.
209 H. Song, Y. Kim, Y. H. Jang, H. Jeong, M. A. Reed and T. Lee, *Nature*, 2009, **462**, 1039–1043.
210 A. S. Blum, J. G. Kushmerick, D. P. Long, C. H. Patterson, J. C. Yang, J. C. Henderson, Y. Yao, J. M. Tour, R. Shashidhar and B. R. Ratna, *Nat. Mater.*, 2005, **4**, 167–172.
211 M. Rahimi and A. Troisi, *Phys. Rev. B: Condens. Matter Mater. Phys.*, 2009, **79**, 113413.
212 B. Xu, X. Xiao, X. Yang and L. Zang, Tao, *J. Am. Chem. Soc.*, 2005, **127**, 2386–2387.
213 D. G. de Oteyza, P. Gorman, Y.-C. Chen, S. Wickenburg, A. Riss, D. J. Mowbray, G. Etkin, Z. Pedramrazi, H.-Z. Tsai, A. Rubio, M. F. Crommie and F. R. Fischer, *Science*, 2013, **340**, 1434–1437.
214 A. Riss, S. Wickenburg, P. Gorman, L. Z. Tan, H.-Z. Tsai, D. G. de Oteyza, Y.-C. Chen, A. J. Bradley, M. M. Ugeda, G. Etkin, S. G. Louie, F. R. Fischer and M. F. Crommie, *Nano Lett.*, 2014, **14**, 2251–2255.
215 J. Lee, S. M. Perdue, A. Rodriguez Perez and V. A. Apkarian, *ACS Nano*, 2014, **8**, 54–63.

 This journal is © The Royal Society of Chemistry 2015